www.itcon.org - Journal of Information Technology in Construction - ISSN 1874-4753

AUTOMATED HAZARD IDENTIFICATION AND ENERGY-BASED RISK ASSESSMENT FOR TOWER CRANE LIFTING OPERATIONS USING RTK-GNSS POSITIONING AND TRACKING

SUBMITTED: October 2025
PUBLISHED: May 2026
EDITOR: Robert Amor
DOI: 10.36680/j.itcon.2026.026

Kepeng Hong, Ph.D. Candidate
Department of Civil and Mechanical Engineering, Technical University of Denmark (DTU)
https://orcid.org/0009-0005-0018-0579
keho@dtu.dk

Jochen Teizer, Professor
Department of Civil and Mechanical Engineering, Technical University of Denmark (DTU)
https://orcid.org/0000-0001-8071-895X
teizerj@dtu.dk

SUMMARY: *Tower cranes are critical for lifting heavy elements in prefabricated and modular construction, but their operations pose significant safety risks. This study proposes a data-driven method using Real-Time Kinematic Global Navigation Satellite System (RTK-GNSS) that tracks the crane trolley and workers movements and assesses the potential struck-by hazards from lifted payloads. By analyzing the trolley's velocity and vertical displacement, the novelty in the method respectively detects the lifting stages and estimates the payload weight, while pairing its real to the planned placement location in the Industry Foundation Classes (IFC) model. An energy-based hazard assessment computes the intensity of detected incidents when workers' RTK-GNSS wearables are inside of hazardous crane swing zones. The severity is evaluated in the form of a statistical analysis and density map. Unprecedented safety-relevant information becomes available to practitioners that can use it in responsible decision-making. Compared to computationally intensive systems such as cameras, the proposed method provides an alternative cost-effective, scalable solution for automating the monitoring of hazardous outdoor workspaces.*

KEYWORDS: *Building Information Modeling, close calls (aka. near misses), crane hoisting, energy-based hazard recognition assessment, construction equipment sweep curves, construction site safety planning and control, gravity and motion energies, proactive safety monitoring and alerting, real-time location sensing, safe workplace environments, safety data visualization.*

REFERENCE: *Hong, K., & Teizer, J. (2026). Automated hazard identification and energy-based risk assessment for tower crane lifting operations using RTK-GNSS positioning and tracking. Journal of Information Technology in Construction (ITcon), 31, 584-613. https://doi.org/10.36680/j.itcon.2026.026*

1. INTRODUCTION

Construction sites have been considered one of the most dangerous workplaces with a high proportion of accidents, accounting for nearly 23% in Europe and 20% in the US of all workplace fatalities (BLS, 2024; Eurostat, 2024). While the tower crane plays an essential role in construction sites because of its capability to lift and transport heavy loads efficiently, operational complexity also makes it a significant contributor to workplace fatalities and injuries. Between 2020 and 2024, 339 crane-related accidents were recorded in the United States (OSHA, 2024).

Among various crane types, 22% of all crane-related fatalities occurred with tower cranes, of which 8% in the European Union (Milazzo et al., 2016). Staying in the context with tower-crane operations, the events most relevant to this study are struck-by incidents caused by lifted or falling loads. The primary causes of these accidents include crane collapses, load drops, equipment failures, and operator errors, where 16% of crane-related accidents were attributed to workers being struck by falling loads from crane jibs, and 2% were linked to mishandling heavy loads. Over half of all fatal crane injuries involve workers being struck by objects or equipment, with approximately 60% of these incidents resulting from falling objects (BLS, 2019).

Despite these risks, effective and automated tower crane monitoring methods to assess hazards and ensure worker safety remain underdeveloped. Traditional safety measures rely on the experience and observation of operators and workers, underscoring the need for more automated and robust approaches that can assist human behavior.

Smart sensing technologies have been widely adopted to automate tower crane monitoring (Ali et al., 2024). The development of sensing systems that provide real-time data on crane status, load weights, and environmental conditions can significantly enhance operational safety. Such systems can provide alerts and feedback to operators and site managers about potential hazards before they lead to accidents. Various sensors, including localization- and vision-based systems, have been implemented to enhance the safety and productivity of tower cranes. These sensors measure parameters such as hook location, slewing angle, and load weight to monitor lifting operations (Danel et al., 2024; Nishizawa & Mishima, 2024; Sacks et al., 2005). However, existing monitoring systems are often integrated into crane operation systems for safety and maintenance, making it challenging to retrieve data for further analysis. And they often depend on multiple devices to achieve robust activity and struck-by hazard identification in lifting operations (Hu et al., 2024).

Hence, a research gap is identified in developing simple yet robust methods for monitoring tower crane operations, enabling the detection of lifting operations and involved hazards, with an explicit emphasis on detecting struck-by hazards from lifted payloads. This study addresses this gap by proposing a method that leverages real-time kinematic global navigation satellite systems (RTK-GNSS) technology to track the spatial movement of the crane trolley. RTK-GNSS enables high-precision positioning and enhances standard Global Positioning System (GPS) accuracy. It uses a static base station to transmit real-time corrections to moving rovers, for example, enabling centimeter-level accuracy for tracking crane motion and load-induced displacement.

The core of proactively avoiding accidents is identifying hazards and detecting incidents at the right time. The criteria for detecting incidents related to dynamic hazards are primarily based on the proximity between pedestrian workers and the dynamic hazards. Concepts such as safety distance and protective envelopes are all variants of proximity-based criteria. However, proximity-based methods do not reflect the potential severity of the incident. Energy-based hazard assessment has existed for decades (Hadden, 1970) and yet recently gained attention again (Fleming & Fischer, 2017) as a reasonable quantitative hazard assessment method when considering hazard severity. In this work, we adopt an energy-based method to assess struck-by hazards involving lifted loads.

This study aims to identify hazards associated with lifting operations and develop an automated method for hazard detection and assessment. Using RTK-GNSS technology to track the lifting operation route allows for identifying lifted prefabricated elements from the as-planned model. Then, the weight and dimensions of lifted elements are determined by analyzing the centimeter-level vertical and horizontal displacements of the trolley during the lifting operation. Hazard energy and hazard zones related to lifted payload are then identified, quantified, and assessed. In summary, based on the identified research gap, we aim to answer the following research questions (RQs):

- RQ1: Can RTK-GNSS sensors alone capture both vertical and horizontal displacements with sufficient resolution to detect lifting operations?
- RQ2: Can vertical displacement be used to estimate the weight of lifted elements, and how can this be validated and enhanced using as-planned models?

- RQ3: How can the integration of crane trajectories with building models be used to identify hazard zones and compute energy-based risk metrics during lifting operations?
- RQ4: Can we use RTK-GNSS data to visualize and quantify the spatial and temporal distribution of struck-by hazard energy and evaluate incident severity when workers are detected in the risk zone?

In addressing these research questions, this study makes two main contributions. First, it proposes an RTK-GNSS-based framework for automated identification of lifting operation stages and prediction of lifted payload properties, enabling quantitative energy-based hazard assessment. Second, it demonstrates that a single RTK-GNSS sensing modality can support multiple monitoring tasks without relying on vision-based or multi-sensor systems, providing a practical and scalable solution for real-world construction environments.

The paper is organized as follows. Section 2 reviews the related work in tower crane operation safety, location tracking technology, crane monitoring technologies, and applications. Sections 3 and 4 present the framework and methods we adopted in this work. Section 5 shows the experimental setup and results to two case studies where we implemented the framework and methods. In the end, we conclude the strengths and limitations of the method based on the case study results.

2. RELATED WORK

This section reviews sensing technologies and hazard assessment methods for monitoring tower crane lifting operations. It first outlines general sensing technologies applied for safety monitoring, then examines data-driven methods for activity recognition, and concludes with energy-based approaches to hazard assessment.

2.1 Sensing technologies for tower crane monitoring

Tower crane monitoring has been extensively studied using a wide range of sensing technologies, including location-based, vision-based, and environmental sensors (Rao et al., 2022; Sherafat et al., 2020). These sensing methods aim to address key challenges in tower crane operations, including safety-related concerns such as collision risks, blind spots, and proximity to workers, as well as productivity issues such as cycle time monitoring and idle time reduction. By providing these insights, the sensors contribute to both operational control and real-time safety management.

A variety of measurement sensors have been integrated into crane operation control systems, including angle sensors, horizontal and vertical trolley displacement sensors, tilt sensors, wind speed sensors, and load sensors (Ali et al., 2024; Zhong et al., 2014). These sensors monitor essential operation parameters for collision avoidance (Fang et al., 2018; Yong et al., 2023) and load verification (Nadar et al., 2013). Moreover, the recorded measurements can be further analyzed to assess operational productivity. For instance, Danel et al. (2024) collected data on load weight and hook height from built-in anti-collision systems to track concrete pouring progress, offering insights into productivity improvements. Nevertheless, data from built-in sensors is often inaccessible, and up-to-date sensor systems may not be available.

To overcome the limited accessibility of built-in sensors, researchers have deployed more advanced sensing technologies to capture multimodal data. First, localization-based sensors, such as GPS and UltraWideband (UWB), are essential tools for enhancing safety and productivity on construction sites by enabling location tracking of workers, equipment, and site resources. Cheng et al. (2011) assessed UWB's performance in resource location tracking, demonstrating its feasibility in monitoring mobile crane operations and identifying fall hazards. To address limited operator visibility, they also developed a model to evaluate crane operator sightlines by applying UWB to track pedestrian movement in hazardous zones (Cheng & Teizer, 2014). Hwang (2012) proposed an approach using UWB tags on crane jibs to detect proximity between jibs and prevent collisions. Fang and Cho (2015) employed an inertial measurement unit (IMU) to monitor load orientation, position, and sway during lifting activities. Costin and Teizer (2015) employed Radio Frequency Identification (RFID)-based tracking to visualize worker locations within a site layout model. Park et al. (2017) integrated Bluetooth Low Energy (BLE) tracking the movement of workers with a Building Information Modeling (BIM) model for safety monitoring in an indoor construction environment. For outdoor environments, GPS-based tracking has also been widely used due to its broad coverage and simplicity. GPS data has also been used for spatiotemporal analysis of construction equipment operations, offering a low-cost solution for automated monitoring (Pradhananga & Teizer, 2013). Enhanced from traditional GPS, RTK-GNSS provides centimeter-level accuracy by utilizing satellite signals and corrections from

static sensors (Wielgocka et al., 2021). In our previous work, RTK-GNSS was tested to track both ground-based equipment and workers on construction sites, supporting the detection and quantification of safety incidents (Johansen et al., 2024a; Hong & Teizer, 2025).

Alternatively, vision-based sensors have gained increasing attention with advancements in computer vision methods. For instance, Yang et al. (2014) developed a vision-based crane tracking system to analyze jib trajectories and tower crane activities. Fang et al. (2018) mounted a camera on the crane to monitor load sway and the dynamic behavior of the payload during lifting tasks. More recently, Chian et al. (2022) demonstrated that detecting lifted payloads from video footage can support the identification of potential fall zones beneath. Given that tower cranes offer an ideal top-down perspective of construction sites, they are often used as camera mounting places for comprehensive visual monitoring of the sites. For instance, Pfitzner et al. (2023) used vision data collected from a crane-mounted system to map worker locations onto BIM floor plans for productivity analysis. In general, positioning accuracy across sensing technologies ranges from meter-level for standard GNSS approaches to decimeter-level for UWB systems and centimeter-level for RTK-GNSS. Table 1 summarizes the typical accuracy and limitations of representative sensing technologies in aforementioned studies.

Table 1: Comparison of sensing technologies for crane monitoring.

Technology	Example studies	Typical accuracy	Limitations
RTK-GNSS	Weldegk et al., 2021	cm-level (absolute)	signal obstruction
GPS	Pradhananga & Teizer, 2013	m-level (absolute)	signal obstruction, atmospheric delay
UWB	Cheng et al., 2011	decimeter-level (absolute)	range / interference
Vision	Fang et al., 2018	cm-level (absolute)	occlusion, lighting sensitivity
IMU	Fang et al., 2018	high relative accuracy, no absolute positioning	drift accumulation, signal interference

The growing adoption of the Digital Twin concept in construction further enables the integration of Internet of Things (IoT) technologies to communicate, process, and fuse multimodal sensor data with contextual information (Sacks et al., 2020; Teizer et al., 2024). Digital Twin provides a platform for supporting comprehensive real-time analysis and proactive intervention in site operations, e.g., integrating real-time load and position data for scenario simulation. Ontologies for safety and productivity on Digital Twin platforms have also been widely studied for efficient data integration of sensors (Speiser & Teizer, 2024a).

2.2 Data-driven methods for activity and hazard detection

Lifting operations are complex processes involving multiple stages, such as rigging, derigging, hoisting, and slewing (OSHA, 2014). Distinguishing between these stages and associating the operations with construction activities is essential for effective lift planning, progress monitoring, and hazard identification (Ali et al., 2024; Hu et al., 2021). Accurate stage recognition can be achieved by analyzing trajectory, orientation, and load data collected by sensors. Data-driven methods have been widely applied to a range of project types, including in-situ concrete casting and prefabricated element assembly. These methods rely on diverse sensor data and are implemented using either rule-based or machine learning techniques.

Rule-based methods use predefined criteria and thresholds, established through domain knowledge and expert input, to differentiate operational stages or identify hazards involved (Johansen et al., 2024b). Trajectory data, such as the slewing angle of crane jibs and the height of suspended loads, has been used as a key indicator. For instance, Sacks et al. (2005) proposed an approach that leverages crane hook location and weight data to segment crane working cycles. Similarly, Danel et al. (2021) segmented lifting operations into six stages—rest, approach, attach, transport, load, unload, and detach—based on the same types of data. More recently, Nishizawa and Mishima (2024) integrated vision data by combining RTK-GNSS with cameras to identify lifting work stages and recognize lifted elements, despite misclassification issues due to the lack of information on payload status. In combination with contextual information (e.g., site layout models), trajectory data is able to provide semantic understanding. Yang et al. (2014) categorized tower crane operations into two main activity types, respectively, concrete pouring and non-concrete material movement, and tracked these activities based on crane jib movement patterns and site layout information. Zhao et al. (2019) integrated data from RFID and Long Range technologies and BIM models to analyze and display real-time information about prefabricated components. High-precision displacement data has also been used to monitor the health of static structures and moving equipment. For instance, Xiong and Niu (2019) employed RTK-GNSS to study the horizontal vibration of high-rise structures. Their approach applied the

Savitzky-Golay method to reduce background noise and used the Fast Fourier Transform to extract dynamic parameters from the displacement signals.

Payload weight data is also critical for operation and safety monitoring, such as preventing overloading and identifying lifting activities. Sensors used for load weight measurement include tensile link, crane scale, load measuring pins, and load cells, most of which measure load weight through strain or compression measurement (Carmona et al., 2019; Zhang et al., 2025). To estimate payload weight, Kusznir and Smoczek (2023) proposed a data-driven approach to estimating the static payload using genetic programming to model the nonlinear relationship between strain data, trolley position, and payload mass in the lab environment.

In contrast to rule-based methods, machine learning methods perform tasks, such as classifying activities and detecting hazardous situations, using models trained on labeled input datasets. Rashid and Louis (2020) used IMU sensor data and k-Nearest Neighbors (KNN) to recognize excavator activities in earthmoving operations, including digging, swinging loaded, dumping, and swinging empty. Jiang and Ding (2024) applied transfer learning on strain sensor data to detect and identify 4 hazardous conditions, including vertical hoisting, tilt hoisting, sudden braking, and sudden unloading, in lifting operations. While machine learning methods show an advantage in adaptability, rule-based methods remain reliable, particularly when training data is scarce.

2.3 Energy-based hazard assessment and control

Many studies have been conducted to quantify and assess safety conditions, hazard potential, and incident severity on the construction site. Lagging indicators, such as the number or rate of injuries, illnesses, and fatalities, are commonly used in safety management. In contrast, leading indicators are increasingly encouraged, as they represent proactive and preventive measures aimed at identifying and eliminating hazards before they result in accidents (Marks et al., 2013; OSHA, 2019). Leading indicators, such as the number of improperly installed guardrails and the number of workers entering the proximity of operating machinery (Hong & Teizer, 2024), can be effective in detecting incidents and evaluating hazard levels. However, most existing hazard indicators remain empirical and qualitative, offering limited ability to quantify the potential impact if hazards lead to incidents. This gap underscores the need for more systematic, data-driven approaches to hazard assessment that incorporate both the likelihood of occurrence and the magnitude of possible outcomes (Ning et al., 2018).

Energy-based hazard assessment and control have been recognized as a scientifically grounded quantitative method. Haddon (1968) first introduced the energy release theory, which connects hazards and potential injuries or fatalities based on physics principles. Building on this foundation, Albert et al. (2014) categorized hazards into ten primary energy sources, including gravity, motion, mechanical, and electrical energy. Recently, Hallowell et al. (2017) analyzed over 500 injury cases and found that higher task energy levels often lead to more severe injuries, identifying energy intensities above 2.56 J/cm^2 (25.6 kJ/cm^2) as high-risk. Specifically for tower crane hazard assessment, Hu et al. (2023) proposed an energy-based hazard taxonomy, including sources like electricity, motion, gravity, and chemicals, and applied it to a live project. In addition, energy-based hazard assessment has also been integrated into safety training through pre-job meetings (Bayona et al., 2025) or a serious game (Speiser & Teizer, 2024b).

Mitigation strategies range from lifting path planning to broader safety improvements, such as site layout optimization and schedule adjustments, to minimize potential hazard risks in lifting operations. Lifting route planning requires robust planning, including maintaining proper clearances, avoiding load movement over workers, and coordinating communications among crane operators and riggers. These plans not only optimize logistics but also prioritize worker safety by avoiding hazardous zones and enforcing clearance buffers (Hu et al., 2021). Visualization and reporting tools also play a crucial role in managing site hazards and supporting proactive safety management. Personalized feedback helps workers and operators better understand risks and adopt safer operations and behaviors. Teizer and Cheng (2015) introduced a proximity hazard indicator to capture and map near-miss locations for monitoring the interaction between workers and equipment. More recently, Golovina et al. (2016) advanced the approach by using heat maps to identify struck-by and near-miss locations, supporting predictive safety planning. Hu et al. (2023) combined path-finding algorithms with 3D heatmaps to quantify and visualize hazard exposure, incorporating factors such as likelihood of occurrence, energy intensity, and spatial impact.

To sum up, current sensor-based hazard identification methods often rely on multiple sensor types to detect lifting operations and typically yield only qualitative results for incident detection and assessment. This study proposes a

data-driven RTK-GNSS-based method to estimate hazard energy in tower crane lifting operations. By analyzing trolley trajectory data, the method identifies spatial hazard zones and quantifies their energy intensity. Vertical displacement data are used to infer payload weight and component dimensions, which are then integrated with the as-designed building model to reduce dependence on multiple sensor inputs.

3. METHODOLOGY

This section presents the novelty of the method that identifies lifts of prefabricated elements and quantifies hazards associated with lifting operations, as illustrated in Figure 1. The method integrates RTK-GNSS data with BIM model through the following steps: (1) extract component information from the BIM model, (2) correlate vertical displacement with payload weight, (3) detect lifting operations via trolley tracking, and (4) identify dynamic hazard zones and potential energy intensity.

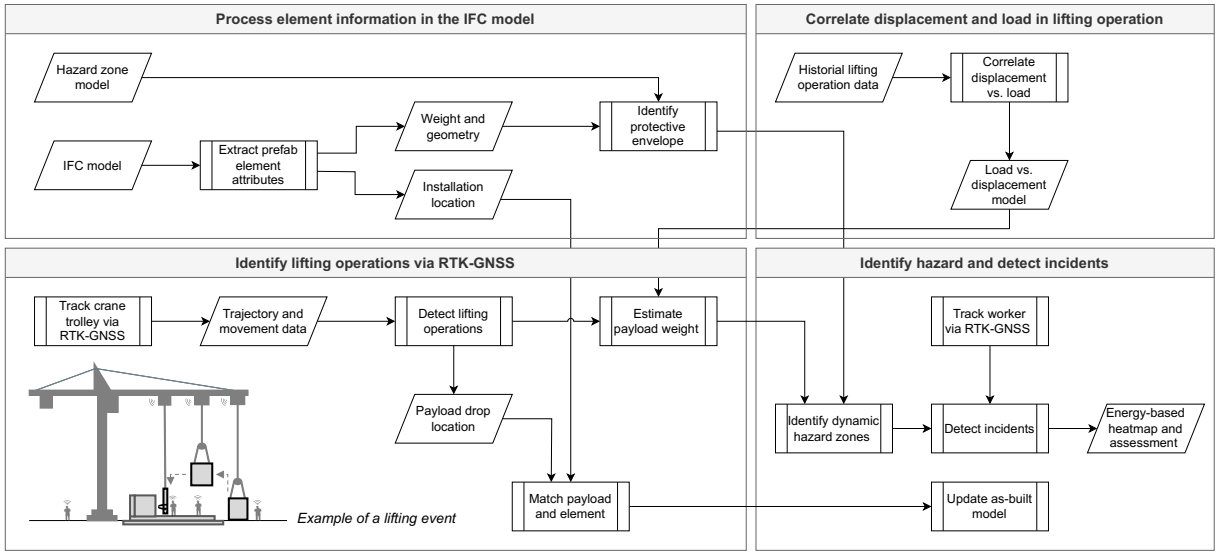

Figure 1: Methods of identifying dynamic hazard zones and detecting incidents for a typical lifting event.

3.1 Installing RTK-GNSS receivers on tower crane trolleys

To capture key crane motions for safety monitoring, the RTK-GNSS receiver must be strategically placed. In this study, an RTK-GNSS receiver is mounted on the trolley, rather than the hook, for better operability (e.g., power supply and network connectivity), while still capturing the movement of the payload.

3.1.1 Understanding tower crane components and operational movement

To facilitate understanding of tower crane motion, an overview of different components in a tower crane is presented in Figure 2. A tower crane consists of multiple mechanical and structural components that handle heavy materials. The key components of lifting materials include:

- Jib: A horizontal beam extending from the tower that supports the trolley and hoisting system.
- Trolley: A carriage that travels along the jib, adjusting the load's horizontal position.
- Turntable: A rotating base that allows the jib to pivot for radial load placement.
- Counterweights: Masses mounted opposite the jib to offset load moments and prevent tipping.

On construction sites, tower cranes lift heavy loads—such as prefabricated elements and concrete barrows—from pickup to assembly locations. The trolley system enables precise load placement through three primary movements:

- Hoisting: Upward and downward movement of the load using a hoist motor, controlled by the tension in the lifting cable and hoist speed.

- Traversing: Linear movement of the trolley along the jib, driven by a trolley motor and pulley system.
- Slewing: Rotation of the jib around the mast via a slewing mechanism.

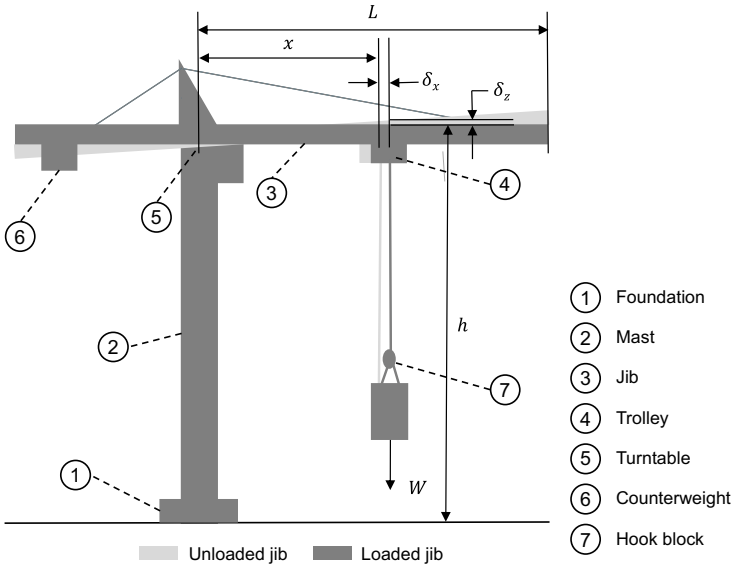

Figure 2: Tower crane component and jib deflection.

Each lifting operation typically involves hoisting, traversing, and slewing. Analyzing trolley movement helps identify both complete lifting cycles and their constituent stages.

3.1.2 Installing RTK-GNSS sensors and preprocessing data

RTK-GNSS consists of a base station and rovers. The base broadcasts correction signals to nearby rovers to reduce measurement errors. In this study, Emlid Reach M2 modules were used as the RTK-GNSS receivers, providing real-time kinematic positioning with centimeter- to sub-centimeter-level accuracy under open-sky conditions. A local base station was deployed on site to provide correction signals to the rover mounted on the trolley. The system operated at a sampling rate of 5 Hz. According to the specification provided by the manufacturer (Emlid, 2024), the Emlid M2 modules can achieve sub-centimeter accuracy in both horizontal and vertical directions, as detailed in Table 2.

Table 2: Positioning accuracy of Emlid M2 RTK-GNSS sensor (as listed in the specification).

Mode	Orientation	Specified precision
Static	Horizontal	4 mm
Static	Vertical	8 mm
Kinematic	Horizontal	7 mm
Kinematic	Vertical	14 mm

Rovers are mounted on the trolley to track vertical displacement (δ_z as illustrated in Figure 2) with high precision, which is used to infer the weight of lifted payload, which is modeled in the following section. Raw data from RTK-GNSS rovers is recorded in WGS84 format (i.e., latitude, longitude, and altitude), which is not directly compatible with the Cartesian coordinate system used in the IFC model. RTK-GNSS data is converted to UTM format (i.e., easting, northing) to allow Euclidean distance calculations. Using a coordinate transformation method from (Hong & Teizer, 2024; Hong & Teizer, 2025), RTK-GNSS data is aligned with the BIM model for spatial analysis of trolley and worker trajectories.

To measure accuracy in both vertical and horizontal directions, 50- and 95- percentile tests were conducted using a 3-hour location distribution from one RTK-GNSS rover placed in a static position. Signal noise, caused by obstructions from nearby structures, was filtered using a simple moving average (SMA), which also reduced oscillation from minor disturbances like wind. SMA was selected for its simplicity and efficiency, making it suitable for on-site, real-time smoothing without prior motion models.

3.2 Analyzing trolley trajectories and crane movement

Understanding trolley and load movement is essential for identifying lifting stages and estimating payload-related structural responses. After lifting the payload to a safe height, the trolley transports it along the jib. The jib shows downward deflection, causing small vertical displacements, which are detectable by the RTK-GNSS sensor. To model the motion of tower crane components, researchers have developed various kinematic and static models (Devesse, 2012; Kang & Miranda, 2004; Rauscher & Sawodny, 2017). Tower cranes are typically treated as underactuated systems with high degrees of freedom (DOF), including jib rotation, trolley translation, hoist movement, and hook rotation. When accounting for the swing of the cable and the lifted load, the system can involve up to eight DOF (Shi et al., 2021). In this study, we simplify the system to focus only on jib deflection during hoisting.

3.2.1 Predicting payload weight

Lifting a heavy payload causes the jib to deflect elastically, resulting in vertical displacement of the trolley, as presented in Figure 3, where examples of polynomial prediction curves are also shown for elements with various weights. Trolley positions vary at the same jib location depending on the payload weight. Two highlighted lifting operations show that heavier loads produce greater vertical displacement. To analyze the relationship between the load weight and the displacement, the jib was modeled as a cantilever beam with the trolley acting as the load point. Dynamic effects such as damping and oscillation are neglected for simplification. This assumption is reasonable for lifting scenarios with relatively stable motions and moderate load variations, where quasi-static behavior dominates. However, in real-world operations involving significant dynamic effects (e.g., large load swings, rapid acceleration or deceleration, or cable flexibility), this simplification may introduce deviations in the estimated load position and weight. Therefore, the proposed approach is primarily applicable to typical lifting conditions with limited dynamic disturbances, and its performance under highly dynamic scenarios requires further investigation.

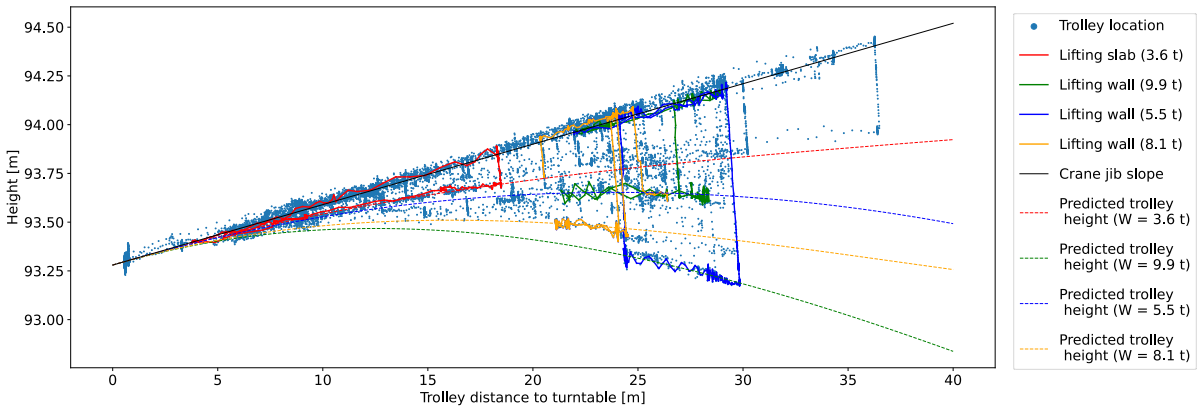

Figure 3: Trolley height vs. distance with measured positions and predicted paths for payloads (note: depicted scale on horizontal and vertical axes are different; crane jib tilts slightly upwards when no payload is attached).

In the simplified physics-based model, the jib can be approximated as a cantilever beam. When lifting a heavy load, the jib undergoes deflection, which can be estimated using the fundamental beam deflection theory from structural engineering. The vertical displacement of the trolley (δ_z) under a load (W) is estimated using the classic cantilever beam Equation (1):

$$\delta_z = \frac{W \cdot x^3}{3EI} \tag{1}$$

where δ_z is the vertical displacement of the trolley (m), x is the trolley distance (m), W is the load weight (N), E is Young's modulus (Pa), and I is the moment of inertia (m^4).

However, the nonlinear behavior of crane dynamics (e.g., payload swing and cable flexibility) makes it difficult to accurately predict lifted weight using a polynomial model, whose accuracy is limited in real-world conditions. Machine learning methods are tested using the same input features. Three models are evaluated: Polynomial Regression, Random Forest, and XGBoost. Polynomial Regression captures the beam deflection relationship and

serves as a physics-informed baseline, while Random Forest and XGBoost are data-driven ensemble methods capable of modeling nonlinear interactions and handling noisy field data (Bishop, 2006). The input features include vertical displacement and trolley distance to the mast, and the output is the estimated payload weight. A 5-fold cross-validation is used for model training and evaluation. Model performance is assessed using the Root Mean Squared Error (RMSE), Mean Absolute Error (MAE), and R^2 score, defined as:

$$RMSE = \sqrt{\frac{1}{n}\sum_{i=1}^{n}(y_i - \hat{y}_i)^2} \tag{2}$$

$$MAE = \frac{1}{n}\sum_{i=1}^{n}|y_i - \hat{y}_i| \tag{3}$$

$$R^2 = 1 - \frac{\sum_{i=1}^{n}(y_i - \hat{y}_i)^2}{\sum_{i=1}^{n}(y_i - \overline{y})^2} \tag{4}$$

where n is the number of observations, y_i is the actual weight value of the lifted load (kg), and $\hat{y}_i$ is the predicted weight value of the lifted load (kg), and $\overline{y}$ is the mean of actual weights (kg).

RMSE and MAE quantify the average magnitude of prediction errors, indicating the average deviation between predicted and actual payload weights, while R^2 reflects the proportion of variance in actual weights explained. The comparative performance of the three models are explained later in more detail (see Table 3). All models are trained with the same input feature set $\{\delta_z,\ x,\ 1/x,\ \delta_z/x^3\}$: measured vertical deflection δ_v, trolley radius x, and two physics-inspired terms. This controls the feature space across methods and isolates model effects. To avoid dynamic effects (e.g., anti-swing and acceleration effect), we detect quasi-static windows where $|\dot{x}| < 0.05$ m/s, $|\dot{z}| < 0.02$ m/s, and $|\ddot{z}| < 0.08$ m/s^2 for over 5s. Within each window we compute δ_v as the median at the same x after removing the unloaded baseline tilt.

Table 3 summarizes the results with 5-fold cross-validation grouped by lift events. XGBoost outperforms the others, achieving the lowest MAE (56.49 kg) and RMSE (246.58 kg), and the highest R^2 score (0.98). Random Forest also performs robustly, with slightly higher errors than XGBoost but comparable accuracy (R^2 = 0.94). In contrast, Linear and polynomial regressions are clearly inferior to field data, indicating that simple parametric forms cannot capture the non-linearities and noise present on site. We therefore adopt XGBoost for online payload estimation, while retaining the regressions as interpretable baselines.

Table 3: Performance of different models of load prediction.

Model	Input features	MAE [kg]	RMSE [kg]	R^2 Score
Random Forest	$\delta_z\ x,\ 1/x,\ \delta_z/x^3$	115.59	428.05	0.94
XGBoost		56.49	246.58	0.98
Linear regression		326.31	864.55	0.77
Polynomial regression (deg = 3)		375.40	1134.43	0.60

3.2.2 Identifying crane lifting stages

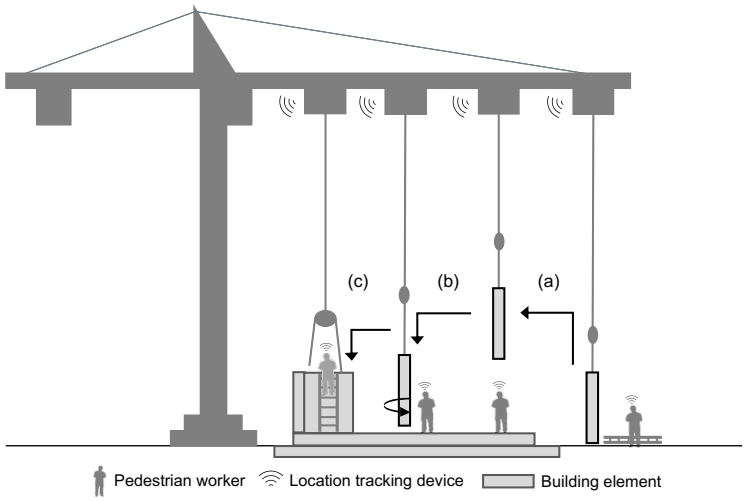

Figure 4: Stages of a lifting operation: (a) hoisting, (b) transportation, and (c) lowering.

A lifting operation involves multiple stages; each associated with distinct hazard types. Figure 4 illustrates an example of a lifting operation, comprising three core stages: (a) hoisting, (b) transportation, and (c) lowering. Additionally, two supplementary stages, attachment and detachment, occur before and after the lift, respectively, with riggers assisting in load handling.

Different stages can be characterized by the trolley's vertical displacement and horizontal movement. Figure 5 presents the height and velocity change of the trolley in a complete lifting cycle. Distinct patterns emerge across stages: zero vertical displacement indicates no load is attached to the hook, while zero velocity reflects stationary periods of the trolley. Six critical time points mark the transitions between key phases of the lifting operation:

- T1: The unloaded trolley arrives at the pickup location, marking the start of the lifting operation,
- T2: The trolley begins to hoist the load as the vertical displacement increases quickly,
- T3: The hoisting stage is completed, and the horizontal movement starts,
- T4: The trolley reaches the target location and begins lowering,
- T5: The lowering process ends as the load is detached,
- T6: The lifting cycle concludes as the trolley leaves the lowering location.

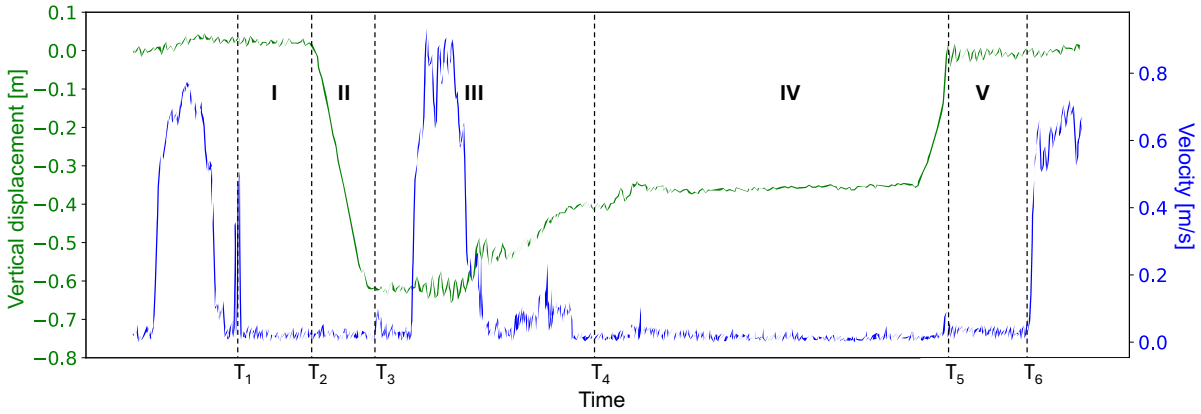

Figure 5: Vertical displacement and velocity changes of a lifting cycle, and identified critical points and stages.

The six time points divide a lifting operation into five stages. In this study, a lifting cycle is defined as the sequence of crane motions associated with transporting a load from the pickup location to the placement location. T1 denotes the time when the unloaded trolley arrives at the pickup location, marking the beginning of the analyzed lifting cycle. Periods before T1 may correspond either to inactive crane states or to unloaded trolley movement outside the analyzed cycle. In tower crane operations, the trolley often remains close to the mast during inactive periods when no lifting task is performed. Table 4 summarizes the classification criteria based on vertical displacement (δ_z) and velocity (v), along with the associated hazards.

Table 4: Classification criteria and hazards of different stages in a lifting operation.

Stage	Description	Involved hazard types	Criteria
I: Rigging	Riggers attach loads to the hook before lifting.	Struck-by hazards due to load flipping	$\delta_z \cong 0$ $v \cong 0$
II: Hoisting	Crane operators begin lifting loads to operational height.	Struck-by hazards due to jib deflection	$\delta_z < 0$ $v \cong 0$
III: Transportation	Lifted loads travel above workers positioned underneath the lifted weight.	Struck-by hazards due to loads falling from height	$\delta_z < 0$ $v > 0$
IV: Lowering	Riggers guide the operator in lowering the load to the assembly location.	Struck-by hazards due to loads falling from height	$\delta_z < 0$ $v \cong 0$
V: Derigging	Riggers detach loads from the hook.	Struck-by hazards due to load flipping	$\delta_z \cong 0$ $v \cong 0$

Based on the defined stages, a rule-based algorithm is developed to identify critical time points, as shown in Algorithm 1. To reduce oscillations caused by damping, load swing, and environmental disturbance, a simple moving average filter with a five-point window (i.e., one second) was applied to smooth the curve. Thresholds for vertical displacement and velocity were set at 0.01 m and 0.05 m/s, respectively. These values were chosen based on the minimum detectable variation from the precision of RTK-GNSS, ensuring sensitivity to actual operational changes. The thresholds also align with observed patterns in the trajectory data, where smaller fluctuations did not correspond to actual stage transitions.

Algorithm 1. Identifying lifting operations and involved stages

INPUT: time-series location data of the trolley
OUTPUT: list of timestamps [t1, t2, t3, t4, t5, t6]
INITIALIZE an empty list of operation stages
SMOOTH the raw data using a simple moving average filter (window = 5 points)
SEGMENT lifting operation using the following criteria:
    Start a segment when either Speed > velocity threshold, or Height difference > vertical displacement threshold
    End a segment when both conditions are no longer satisfied
FOR each identified operation segment:
    SPLIT into sub-stages:
        Loaded phase: Vertical displacement < threshold (shortest duration: 5s)
        Moving phase: Speed > threshold (shortest duration: 5s)
    EXTRACT event times:
        t_1: Start time of operation
        t_6: End time of operation
    EXTRACT times for:
        t_2, t_5: Loaded phase start & end
        t_3, t_4: Moving phase start & end
RETURN [t_1, t_2, t_3, t_4, t_5, t_6]

We evaluate the detector at the event level by aligning each video-annotated lift with the detected time intervals. A video-annotated lift that is detected is a true positive (TP); a detected lift with no corresponding video annotation is a false positive (FP); and a video-annotated lift missed by the detector is a false negative (FN). We report Precision, Recall, and F1 score.

3.2.3 Integrating building and site layout models

As-planned building models include precise data on the geometry, location, and weight of prefabricated elements. These attributes are essential for hazard energy quantification, particularly the element's weight and dimensions. To improve the robustness of estimating the dimensions, the prefabricated elements are grouped into weight classes using 500 kg intervals.

IfcOpenShell (2024), an open-source Python library, is used to extract element attributes. To approximate the spatial envelope of each element, rectangular cuboid bounding boxes are applied, defined by dimensions (D_1, D_2, D_3), which are calculated from the minimum and maximum x, y, and z coordinates. This method is suitable for most prefabricated components that typically have rectangular cuboid shapes, such as slabs, beams, and wall panels. For irregular elements, such as staircases or custom façades, the bounding box may overestimate actual size. However, this approximation avoids underestimating hazard zones generated from element envelopes.

To identify the lifted element in the as-planned building model, a proximity-based approach is employed. It is assumed that the hook, trolley, and centroid of the element align vertically, sharing the same 2D coordinates. However, in practice, minor offsets and overlapping footprints in the IFC model can lead to inaccuracies. To address this, Algorithm 2 iterates through all prefabricated elements installed at the same height and calculates their 2D distances to the trolley location. The element with the closest centroid to the trolley location is identified as the lifted element. A threshold was applied to filter out the elements whose centroids are located more than 3 meters away from the trolley. The 3-meter threshold was selected based on the longest edge of all elements in the IFC model.

IFC element matching is performed exclusively from the installation location. Estimated weight is not used in matching to keep it independent for subsequent validation against IFC mass. If a substantial difference between estimate and element weight is observed, the IFC mass is used for sequential hazard energy potential assessment.

Algorithm 2. Identifying lifted elements based on trolley trajectory

INPUT: Trolley location at lowering stage ($x_{trolley}$, $y_{trolley}$), List of prefab elements ([E_1, E_2, …, E_n]) from the as-planned model.
OUTPUT: Identified prefab element $E_{identified}$

INITIALIZE a list D to store the distance between the trolley location and each prefab element centroid
FOR each prefab element (E_i) in the IFC model:
    EXTRACT the list of vertex coordinates (x_j, y_j, z_j) of the prefab element
    COMPUTE the centroid (x_c, y_c) for the element's footprint polygon
    COMPUTE the 2D Euclidean distance between the trolley location ($x_{trolley}$, $y_{trolley}$) and the centroid (x_c, y_c)
    STORE the element ID and its distance in D
IF the minimum distance in D > 3 m:
    RETURN NULL (No matching prefab element identified)
ELSE:
    Identify the element with the smallest distance $E_{identified}$ = argmin(D)
RETURN Identified prefab element $E_{identified}$

3.3 Identifying and assessing energy-based hazard zones

Energy-based hazard assessment is a quantitative approach for evaluating safety risks on construction sites. In crane operations, lifted payloads present significant struck-by hazards to workers and objects beneath or nearby. The primary hazard energy stems from two sources: gravitational potential energy (E_p) and kinetic energy (E_k) gained during lifting operations. The hazard zone is defined as a dynamic spatial envelope surrounding the payload, within which personnel or equipment may be exposed to hazard energy. The size of hazard zones is determined by the payload's physical characteristics (e.g., dimensions, shape, and mass distribution) and dynamic factors, such as trolley velocity and potential swing motion.

During lifting, we compute provisional hazard energy and zones using (i) deflection-estimated weight classes and (ii) conservative envelopes drawn from an IFC-derived catalogue to support real-time alerting. After placement, we identify the element installation location and then finalize the computation with IFC mass and exact geometry.

3.3.1 Hazard energy assessment

As summarized in Table 2, different lifting stages present varying hazard types. During hoisting, heavy payloads induce structural deflection in the jib and mast (Sacks et al., 2005). This deflection causes horizontal displacement of the payload and introduces struck-by hazards to nearby riggers and equipment. The associated kinetic energy can be substantial due to the high mass of prefabricated elements. This hazard is often underestimated and mitigated informally through rigger experience. For example, an 8.2-ton element exhibited a horizontal movement exceeding 0.5 m due to jib deflection. Despite the moderate velocity (0.1 m/s), the resulting kinetic energy reached 41 kJ, exceeding the 10–20 kJ threshold associated with severe or fatal injuries in struck-by incidents (Hu et al., 2023; Breloff et al., 2023).

The hazard with the highest energy potential is payload drop during transport. The total energy combines gravitational potential, which is based on the vertical distance between the payload and its possible landing footprint, and kinetic energy from the trolley's movement. To ensure clearance, regulations and manufacturer guidelines recommend lifting the load at least 2–3 meters above any obstacles (ASME, 2012). On the other hand, to minimize the potential energy and reduce the impact zone in case of a fall, the load should also be kept as close to the ground as safely possible (FEMA, 2008). For hazard energy estimation, a minimum of 3 meters of clearance is assumed.

The total hazard energy, applicable to all stages of the lifting operation, is calculated to reflect both static and dynamic risks throughout the payload's movement. This includes the risk from gravitational height during hoisting, and the added kinetic energy as the trolley travels, as follows:

$$E_{hazard} = \frac{1}{2}mv^2 + mgH \tag{5}$$

where E_{hazard} is the total hazard energy (J), v is the velocity of the crane trolley (m/s), m is the mass of the payload (kg), and H is the vertical clearance to the nearest surface below (m). Energy losses from friction, air resistance, or elastic deformations are neglected.

3.3.2 Hazard zone identification

Hazard zones are defined as the risky areas directly underneath or adjacent to a suspended payload. During lifting, sway and rotation introduce unpredictable movement, expanding the potential impact zone. If a detachment occurs

during transportation, the fall trajectory and impacting area depend on both its geometry and the rigging configuration, i.e., floor elements are typically hoisted using multiple lift points with balanced rigging, resulting in relatively stable and predictable trajectories. On the other hand, wall panels and irregular-shaped components are often suspended from fewer lift points.

Given that the falling motion of the payload is highly stochastic, each payload is approximated as a rectangular cuboid bounding box defined by dimensions (D_1, D_2, D_3), where $D_1 > D_2 > D_3$, as illustrated in Figure 6(a). The maximum footprint of this simplified envelope defines the worst-case potential impact area. Once the payload has been suspended by the crane, jib deflection contributes to its unpredictable movement, as safety regulations recommend that workers remain clear of the load (Sacks et al., 2020; ASME, 2012).

Figure 6(b) illustrates the hazard zones surrounding the payload caused by jib deflection. While no specific quantitative clearance is defined, the requirement is based on maintaining a safe distance within the foreseeable struck-by hazard zone. A commonly adopted guideline in the industry is to maintain a 3-meter (10-foot) radius around payloads when the height of the load is below 4.5 m (FEMA, 2008). The radius of this hazard zone is determined by the largest edge of the payload D_1, combined with the potential horizontal displacement (d_h) and swing (R_s) induced by the jib's deflection. A freely falling object from height H takes a time of $\sqrt{2H/g}$. Thus, the maximum possible hazard zone radius R_h is given by:

$$R_h = v \cdot \sqrt{\frac{2H}{g}} \tag{6}$$

where:

- R_h is the maximum possible horizontal hazard zone radius (m),
- v is the horizontal velocity of the crane trolley (m/s),
- g is gravitational acceleration (9.81 m/s²),
- H is the vertical clearance to the nearest surface below (m).

After the payload is lifted higher than 4.5 m from the ground, the struck-by hazard zone, also known as the fall zone, is defined as the area where partially or fully suspended materials could reasonably be expected to fall (ISO, 2005). This area is influenced by the load's height, geometry, and swing dynamics. To estimate the maximum impacting radius, the payload is modeled as a point mass at the centroid of the payload in a pendulum system, as shown in Figure 6(c). In the most severe case, then the trolley (traveling at velocity v) stops abruptly, the load behaves like a pendulum of Length L, generating a sway radius v^2/g on top of the horizontal drift.

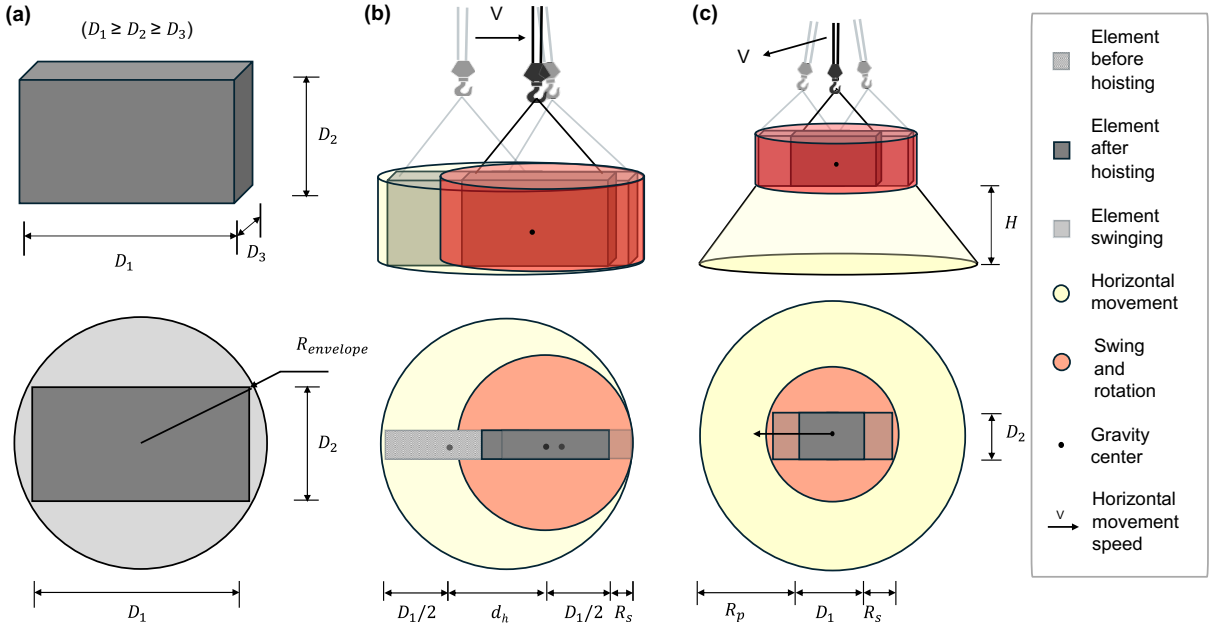

Figure 6: Identified hazard zones related to crane hoisting of a prefabricated element: (a) geometry and projected drop footprint, (b) zones affected by jib deflection, and (c) zones affected by payload drop.

Thus, the maximum possible hazard zone radius R_h combines sway radius R_s and horizontal drift during fall R_p, resulting in:

$$R_h = R_s + R_p = \frac{v^2}{g} + \frac{v^2}{\sqrt{gL}} \cdot \sqrt{\frac{2H}{g}} = \frac{v^2}{g}\left(1 + \sqrt{\frac{2H}{L}}\right) \quad (7)$$

where:

- R_h is the maximum possible hazard zone radius (m),
- v is the velocity of the crane trolley (m/s),
- g is gravitational acceleration (9.81 m/s²),
- L is the vertical cable length,
- H is the vertical clearance to the nearest surface below (m).

A 3-meter buffer is included as per regulatory guidelines (ISO, 2005; OSHA, 2014). Table 3 summarizes hazard zone radius across lifting stages.

Table 5: Dimensions of hazard zones identified in different stages of lifting operations.

Stage	Radius of hazard zone	Description
I: Rigging	$R_h = 3$ m	Static safety buffer zone to protect personnel during rigging
II: Hoisting	$R_h = v \cdot \sqrt{\frac{2H}{g}} + 3$m	Horizontal movement and swing from the jib deflection
III: Transportation	$R_h = \frac{v^2}{g}\left(1 + \sqrt{\frac{2H}{L}}\right) + 3$ m	Load swing during crane travel, with extra buffer for wind and inertia
IV: Lowering	$R_h = v \cdot \sqrt{\frac{2H}{g}} + 3$m	Same as hoisting stage
V: Deigging	$R_h = 3$ m	Static safety buffer to protect personnel during derigging

3.3.3 Hazard energy intensity and incident assessment

To evaluate site safety conditions and assess potential incident severity, this study calculates hazard energy intensity $I(x,y)$ at the location (x,y), representing the spatial concentration of hazard energy across hazard zones. A hybrid function is adopted, where a uniform distribution is assumed within the hazard zone radius, and a Gaussian gradient is applied in the surrounding buffer zone to simulate the energy dissipation. Once the hazard energy E_{hazard} and the hazard zone radius $R_{envelope}$ are determined, the intensity $I(x,y)$ is computed as:

$$I(x,y) = \begin{cases} \frac{E_{hazard}}{\pi \cdot {R_h}^2}, & r < R_h \\ \frac{E_{hazard}}{2\pi\sigma^2} \cdot e^{-\frac{(r-R_h)^2}{2\sigma^2}}, & r \geq R_h \end{cases} \quad (8)$$

where:

- $r = \sqrt{(x - x_0)^2 + (y - y_0)^2}$ is the radial distance from the payload's center (x_0, y_0),
- $I(x,y)$ is the hazard energy intensity (kJ/m²) at the location (x,y),
- E_{hazard} is the total hazard energy (kJ) from the payload,
- σ is the standard deviation controlling the Gaussian decay, which is set to 3 m for the buffer zone,
- R_h is the radius of the hazard envelope zone (as defined in Table 5).

This time-integrated value of worker energy exposure during an incident estimates incident severity, and the maximum instantaneous energy intensity exposure can also be compared with injury risk thresholds. To assess individual daily safety performance, cumulative exposure is calculated for each worker throughout the day.

In addition to evaluating the individual incidents, the intensity level is used to evaluate the spatial distribution of the hazard energy. The construction site is discretized into a uniform spatial grid, where each cell represents a fixed area (e.g., 0.5 × 0.5 m²). For each time interval Δt, the intensity $I(x,y,t)$ during the interval $[t, t + \Delta t]$ is assigned to the corresponding cells within or near the active hazard zones. Over time, it yields a spatiotemporal map of total hazard energy exposure per grid cell. High cumulative values reveal a persistently hazardous location to guide mitigation measures, such as altering lift paths and rescheduling during low site occupancy.

4. RESULTS

A case study was conducted at a residential building construction site in Helsinki, Finland, where a seven-story building was built using prefabricated elements. This section presents the results of applying RTK-GNSS tracking and the proposed data-driven method for detecting lifting operations and evaluating hazard energy intensity throughout the construction process.

The construction site layout is illustrated in Figure 7a, showing designated zones for material storage, concrete pumping, truck unloading, driveways, and lifting radius. The tower crane had a height of approximately 50 meters from the ground, with a jib radius of 40 meters and a counter-jib radius of 22.6 meters. At the time of implementation, the project was in its early stages, with only the ground floor structure under assembly, as shown in the site photo in Figure 7b. Since the BIM model lacked detailed site layout information, the surroundings were approximated as a flat plane with manually defined zones (Figure 7c), which was projected onto a 2D plane (Figure 7d) for integration with trajectory data. The initial as-built model was manually created by combining the as-planned BIM model with on-site observations. Site zones such as walkways, storage areas, and workspaces were defined based on visual inspection of the construction site and drone images. The purpose of this model was to facilitate the identification of crane lifting areas and their relation to construction progress.

During the data collection campaign, multiple struck-by hazards and near-miss incidents were observed, including instances where payloads passed directly over workers or where riggers physically interacted with unstable prefabricated elements. These safety concerns are documented in Figure 8.

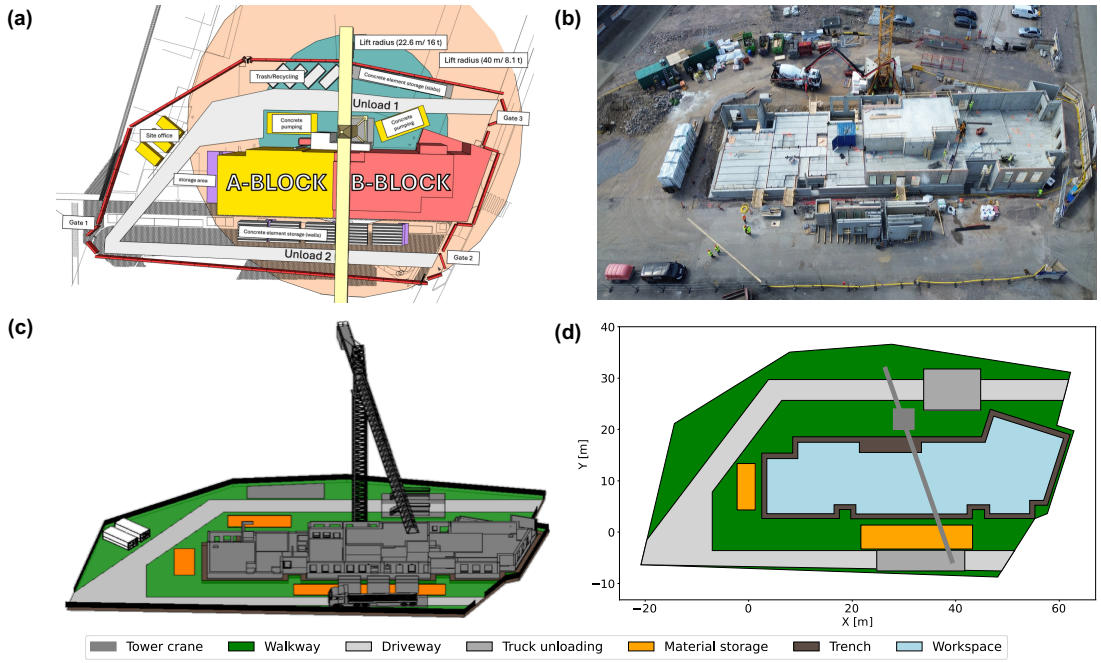

Figure 7: As-built status at the start of the data collection campaign: (a) printed construction site layout, (b) drone-captured aerial view, (c) as-built model, and (d) extracted 2D site layout.

Workers' location data were collected over three days to analyze interactions with the crane, while the crane's operational data were collected and stored on a cloud platform for one month. The raw RTK-GNSS data included the trolley's latitude, longitude, and height, which were transformed to align with the site layout model coordinate system. The height measurements are referenced to mean sea level. An example of the processed RTK-GNSS data is presented in Table 6.

For validation, a static positioning test was conducted by placing a rover in an open area on the ground and recording 10,800 location points over three hours. Accuracy was assessed by computing the deviation from the mean position. On the horizontal plane, the 50th percentile precision was 1.13 cm, and the 95th percentile was 2.34 cm. In the vertical direction, the 50th percentile precision reached 1.02 cm, and the 95th percentile reached 3.21 cm, as shown in the 50th and 95th percentile error plot in Figure 10. These results confirm that the system consistently achieves centimeter-level accuracy in both horizontal and vertical directions.

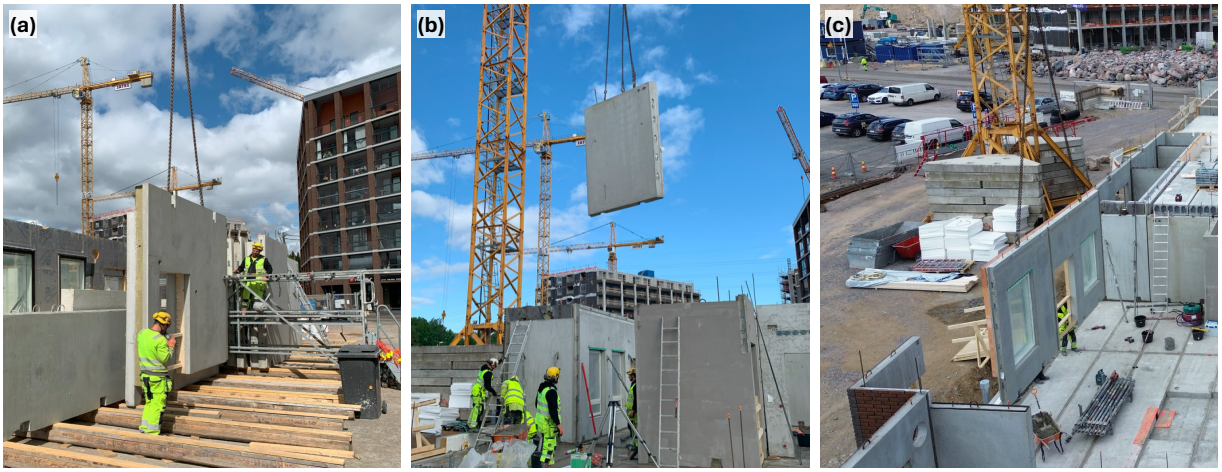

Figure 8: Lifting stages and associated struck-by hazards captured on site: (a) jib deflection during hoisting, (b) payload passing over active work area, and (c) load rotation during lowering.

Figure 9: RTK-GNSS and camera sensors on the crane trolley (left) and embedded in workers' safety vests (right).

Table 6: Example of collected and processed RTK-GNSS data related to the moving crane trolley.

ID	Collected				Processed	
	Consecutive date and timestamp	Longitude	Latitude	Height [m]	X [m]	Y [m]
…	…	…	…	…	…	…
Trolley	2023-05-30 09:40:27.00	60.218995	24.927357	94.115	4.040	17.310
Trolley	2023-05-30 09:40:27.04	60.218997	24.927353	94.107	4.333	17.420
Trolley	2023-05-30 09:40:27.06	60.218999	24.927349	94.087	4.634	17.534
Trolley	2023-05-30 09:40:27.08	60.219001	24.927345	94.073	4.932	17.643
Trolley	2023-05-30 09:40:28.00	60.219003	24.927341	94.060	5.246	17.760
….	…	…	…	…	…	…

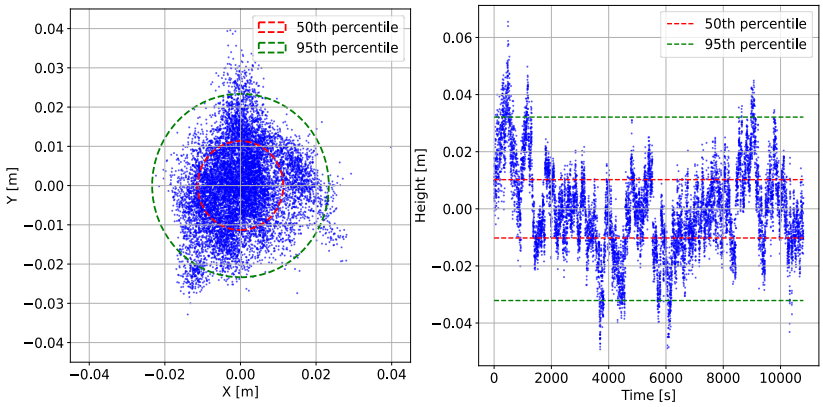

Figure 10: Static RTK-GNSS positioning error on ground level: horizontal distribution (left) and vertical deviation over time (right).

4.1 Identification of lifted elements in the as-planned IFC model

The as-planned IFC model is utilized to support the identification of lifted prefabricated elements, as displayed in Figure 11. The model contained the property data of prefabricated elements, including IfcWall, IfcFooting, and IfcSlab, with detailed data on each element's location, weight, ID, dimensions, and geometries. During the data collection campaign, wall and slab elements were primarily subject to lifting operations since the foundational elements had already been installed. The properties of these elements were extracted from the model and systematically stored in a relational database to enable further classification and weight mapping analysis.

The prefabricated elements were classified into 0.5-ton weight classes. Figure 12 shows the distribution of elements by weight class (left) and the corresponding envelope radius (right). The majority of elements weighed less than 5 tons. The hazard radius for each class was conservatively estimated as half the diagonal of the largest face of the element's bounding box. This accounts for all possible orientations during lifting, providing a safety buffer in the event of a fall. Heavier elements generally correspond to larger envelopes. These values were used to define hazard zones per payload class.

Figure 11: IFC model of the complete building structure: (a) front view and (b) top view.

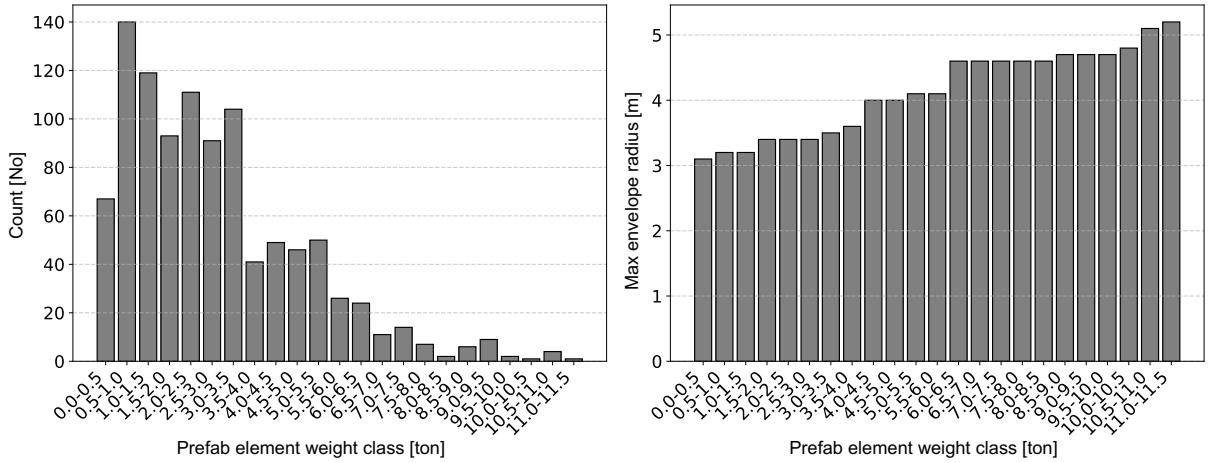

Figure 12: Summary of prefab elements extracted from the IFC model: count (left) and maximum envelope diagonal length (right).

4.2 Detecting lifting operations and associated stages

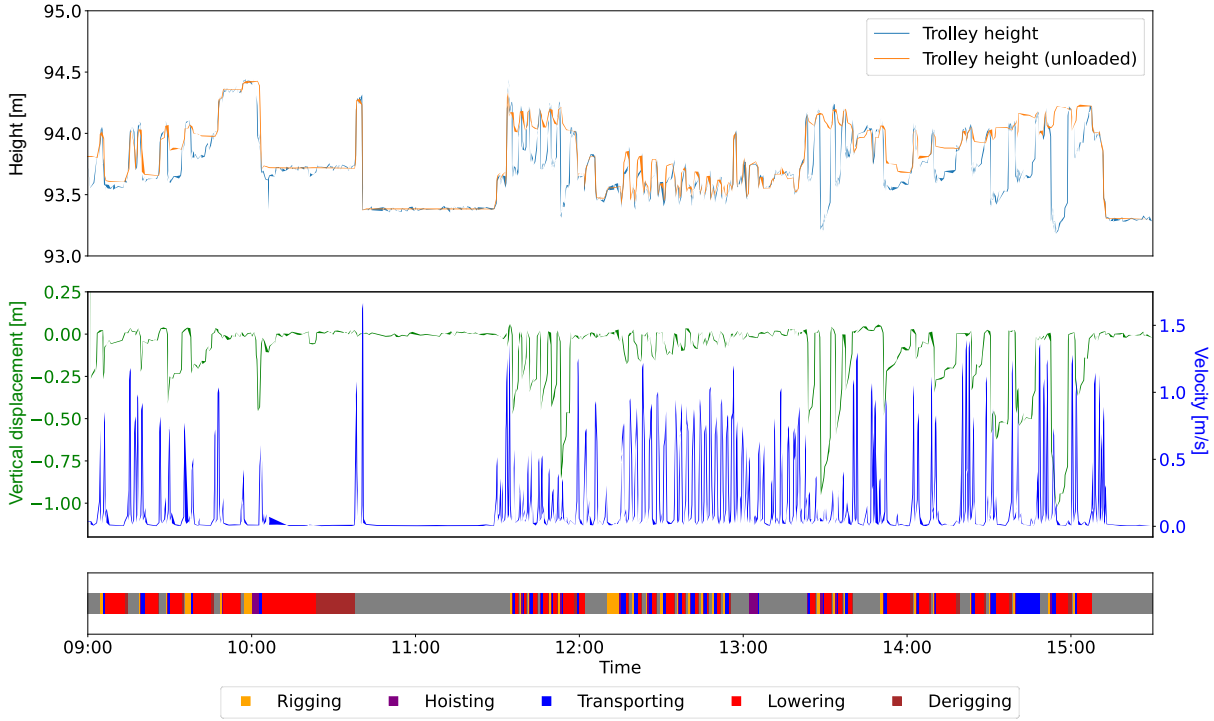

Figure 13: Results of stage identification for one selected day: trolley height change between the loaded and empty states (top), vertical displacement and speed of the trolley (middle), and timestamps of detected lifting operations along with their corresponding stages (bottom).

The rule-based algorithm was implemented to detect lifting operations and identify the various stages. Figure 13 presents the results of lifting operation detection for a single day, identifying 40 distinct lifting events. Video recordings were used to validate the detection results, confirming the identified operations. However, missed detections were observed, particularly between 13:00 and 13:30. Video footage showed that these missed operations involved the lifting of lightweight materials, such as guardrail boards and poles for fall protection installation. Due to their minimal weight, the lifting of these materials resulted in negligible height changes, making them indistinguishable from idle states. This highlights the current limitation of the method in detecting lightweight payloads.

We aligned the rule-based detections with video-annotated events. Across 89 annotated lifting operations, the detector correctly identified 59. For prefab-element lifts, 56/64 were detected. No false positives were observed. Precision, recall, and F1 score are reported in Table 7. Missed detections occur mostly in lightweight lifting (e.g., wheelbarrows, guardrail poles, boards and equipment), which produce deflection below the quasi-static thresholds. This is a limitation of the current rule-based approach. Such operations can still pose safety risks despite their lower mass, and performance can be improved by fusing additional signals, e.g., hook-mounted location sensors.

Table 7: Detection performance of lifting operation identification (precision, recall, and F1 score).

Category	Precision	Recall	F1
Overall	100%	66.30%	79.70%
Prefab elements	100%	87.50%	93.30%

The identification of different stages provides insights into the average duration and variability of the lifting operations. On average, a complete lifting operation took approximately 5 minutes, with durations varying from 134 to 679 seconds. Table 8 provides descriptive statistics of the durations of the detected lifting operation stages, which helps identify stages with longer exposure times and higher variability that may contribute to safety risks. Among the stages, lowering was the most time-consuming and variable, with a mean duration of 154.0 seconds and a standard deviation of 118.6 seconds. This is likely due to the need for precise placement and safety precautions near ground level. Similarly, transporting also showed high variability (mean: 97.7 s; standard deviation: 43.2 s), influenced by crane path length and site layout constraints. In contrast, hoisting was the shortest and most stable stage (mean: 3.7 s; standard deviation: 2.4 s), while rigging and derigging were moderately timed (around 25 s each) with relatively low variation, reflecting standardized procedures. From a safety perspective, the lowering stage poses the highest risk due to prolonged worker exposure and close proximity to suspended loads, particularly when spatial constraints necessitate entry into the hazard zone beneath the load. Transporting also contributes to risk due to possible load sway and dynamic crane movement.

4.3 Identifying lifted elements and updating as-built status

The trolley locations recorded during the derigging stage were used to estimate the final assembly positions of lifted prefabricated elements. Figure 14 shows the spatial distribution of 40 detected lifting operations across the site on one workday. While most activities occurred within the planned site boundary, a few (operations 38, 39, and 40) extended beyond it, reflecting temporary site expansion for fence relocation.

Table 8: Statistics of the lifting operation and its individual stages (in seconds).

Metric	Duration [s]					
	Rigging	Hoisting	Transporting	Lowering	Derigging	Total operation
Min	7.0	1.0	6.0	13.0	1.0	134.0
Max	49.0	9.0	211.0	401.0	87.0	679.0
Mean	24.9	3.7	97.7	154.0	25.2	297.5
Median	24.0	3.0	89.0	86.0	16.0	218.0
Standard deviation	10.1	2.4	43.2	118.6	21.7	157.4

Over half of the lifts were moving prefabricated walls and slabs from the material storage zone to assembly locations. Many operations were concentrated in the lower site area between the material storage and truck unloading zones. In this area, wall elements were first unloaded from delivery trucks, temporarily stored in the material storage zone, and then lifted for final assembly. At the other truck unloading zone, floor and slab elements were lifted directly from delivery trucks to assembly locations. These findings can facilitate improving logistics, such as synchronizing truck deliveries with crane availability and reducing overlaps with worker-occupied zones to improve both safety and efficiency.

Based on the derigging locations, Algorithm 2 was applied to match the lifted elements to their respective IFC model entries. Out of the 40 detected operations, 21 were identified as lifting prefabricated elements. Table 9 lists the 21 identified elements, including their element types, IDs, lifting times, weights, and dimensions. The identified prefabricated elements consisted of two types. The lifting operations occurred throughout the workday, from early morning to late afternoon.

The detailed element-level information enables the site managers to monitor the project progress and update the as-built status of the element, as shown in Figure 15. A total of 21 elements were installed on the first day, followed by 24 on the next. When a lifted element was identified, it was added to the as-built model. The updated as-built model allows for calculating safe hoisting heights for subsequent lifts.

Table 9: Identified lifted elements on one workday.

Element type	Element ID	Lifting time [HH:MM: SS]	Weight [kg]	Dimensions (H×W×L) [m]
Ifcwall	1tmk9dl8r6afbk4rxotztb	09:14:30	2320	3.08×0.16×1.88
Ifcwall	1eyfgjjrp5r8$mgmr3w0ko	09:26:07	3503	3.08×0.20×2.28
Ifcwall	09FA$ibov73xe77uvgiyor	09:35:09	5291	3.08×0.20×3.43
Ifcwall	3cvaoz4gz1b8kx$R_mgtgv	09:46:14	2263	3.08×0.18×1.63
Ifcbeam	3s$tcs0ll6s9luuwfmyuok	10:37:44	3602	0.37×6.08×1.20
Ifcbeam	1pqez6p6dbwoswyog1ukt8	12:18:10	3602	0.37×6.08×1.20
Ifcbeam	0uwbsupf5dxv7jscgjeemo	12:22:55	3602	0.37×6.08×1.20
Ifcbeam	3ogx9skm19pb8jv6s6f5kf	12:28:11	3602	0.37×6.08×1.20
Ifcbeam	3s$tcs0ll6s9luuwfmyuok	12:34:46	3602	0.37×6.08×1.20
Ifcbeam	1pjcpzoclbvhlhroxxaxaj	12:38:54	3602	0.37×6.08×1.20
Ifcbeam	231pu3mdldnvjxohnt8r$k	12:43:42	3602	0.37×6.08×1.20
Ifcbeam	0$Yq06Os9Cdvj1wU7zYPy4	12:47:31	3602	0.37×6.08×1.20
Ifcbeam	3Nnu1kNqHF3gnFLrlWlJoP	12:51:40	3602	0.37×6.08×1.20
Ifcbeam	0eb_usotff7o5iavtumq67	12:55:26	5911	3.48×6.38×0.16
Ifcwall	2pzdifkfh6eauwofxdlhwz	14:02:00	2529	3.48×2.71×0.16
Ifcwall	3bahn85iffieke09cnfcpy	14:08:39	3137	3.08×0.16×3.26
Ifcwall	32a1rpkjh9dqf1dphkzv$9	14:19:24	1397	3.16×1.97×0.10
Ifcwall	2qv1fvbpl5j8ibb7joipew	14:28:45	2877	3.16×6.01×0.10
Ifcwall	0tmjvhfsxethpd0mzga8cl	14:38:09	4452	3.13×0.16×3.55
Ifcwall	2hjpkvuzdbrbeq$gcpxme6	15:00:13	8001	3.13×0.16×6.38
Ifcwall	0$lhtpqgt3lhl5jahoqjol	15:07:39	3123	3.48×3.96×0.16

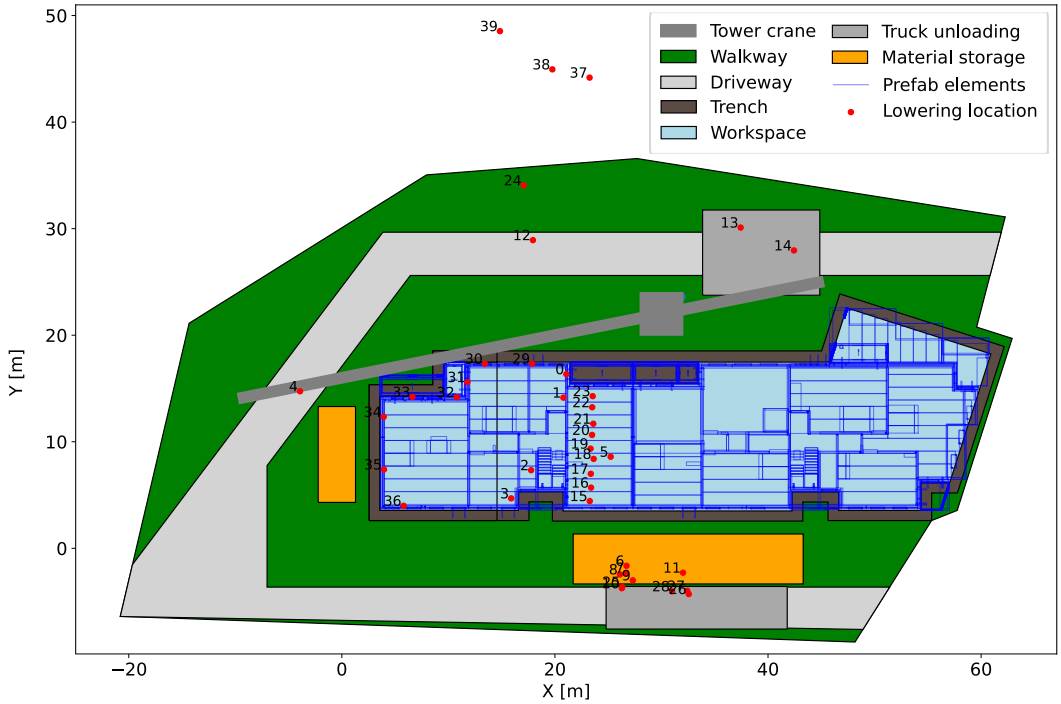

Figure 14: Identified derigging locations of lifting operations on one workday.

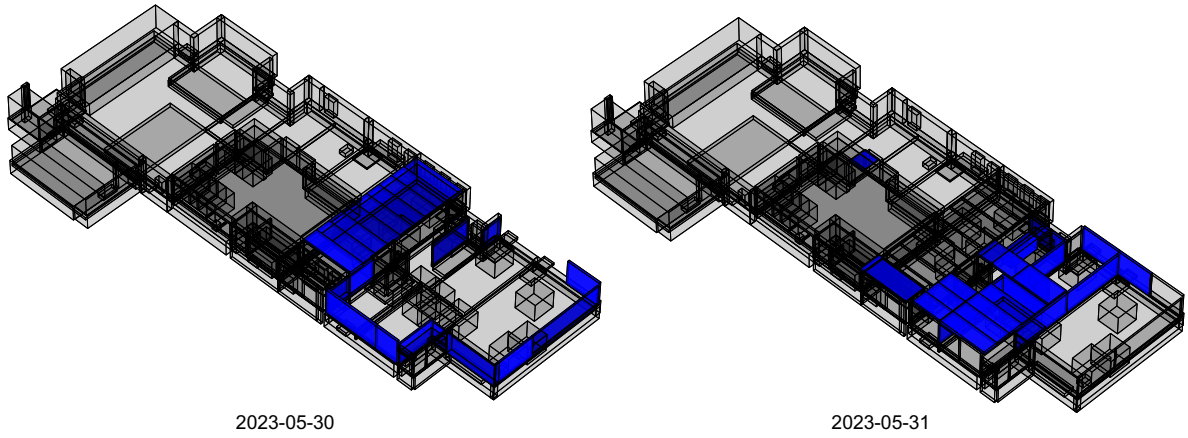

Figure 15: IFC model showing lifted elements (blue: newly installed; grey: as-built) on two days.

4.4 Predicting payload weight and hazard zones during lifting

To enable the real-time hazard zone estimation during the lifting operations, we applied a XGBoost model to predict the payload weights from the vertical displacement data. This resulted in estimated the envelope radius and hazard energy of the lifted payload. The model was trained on 71 lifting operations, using 93,298 data points of vertical displacement and jib position. The predicted weights align well with the actual values, and the RMSE is 246.58 kg, which is below the interval threshold, supporting reliable classification into 500 kg intervals. The predicted load weight allows for the inference of the load envelope dimension, thus helping determine the hazard zones surrounding the payload. However, some loads, such as concrete wheelbarrows or guardrails, are not prefabricated elements and thus lack associated IFC data. For these items, weight-dimension correlations could not be validated. However, their estimated values were still applied for hazard zone estimation, as such loads are typically under 1000 kg and have smaller hazard envelopes than prefabricated components. The result of weight prediction can be validated directly after the completion of the lifting operation by identifying the element in the IFC model. Table 10 presents a validation result of predicted weight classes. The result demonstrates that the predicted weight classes accurately encompass the actual measured weights for all listed elements.

Table 10: Validation of predicted weight class vs. actual weight of lifted payload.

Element ID	Weight [kg]	Dimension [m]	Predicted weight class [kg]	Envelope radius $R_{envelope}$ [m]
2D7heAG8D3$eCekixsoqvj	1371	0.2×1.2×2.5	1000-1500	3.2
2EauZCKtf54OxKJ_ryhl9Q	3346	0.2×3.5×4.1	3000-3500	3.2
3_GGremPr8W9QOMOt_7t7e	3998	0.2×3.5×4.5	3500-4000	3.5
0z4mTGZ3XE0PGTLnfKiS7Q	6577	0.2×3.1×5.0	7000-7500	4.6
3BuFjh4Gz8tePKHrWAO0ip	3463	0.2×2.3×3.1	3000-3500	3.5
3jDk6GrB153BVc5g1NEa7X	7636	0.2×3.1×5.0	7000-7500	4.6
1uiAsyGa93yh6UvV8fVWAp	2056	0.4×1.2×3.5	2000-2500	3.4
1vLnzc79n9kfMK2Jk0sG2u	1371	0.2×1.2×2.5	1000-1500	3.4
0upJsvXPz1WhgIFRttIVP0	3300	0.4×1.2×5.6	3000-3500	3.4

With the determination of load weight and dimensions, estimating the hazard energy during lifting operations also requires knowledge of the vertical clearance and fall height. This study assumes a minimum clearance of 3 meters above any structure along the lifting route. Figure 16 illustrates how vertical clearance, hazard zone radius, and hazard energy intensity evolve during one lifting operation. Sudden drops in vertical clearance reflect variations in the height of the structures beneath. As the payload rose, both hazard energy intensity and the radius of the hazard zone increased beneath it. The majority of the hazard energy potential was attributed to the elevated height of the load, while only a small portion resulted from kinetic energy. This real-time estimation is essential for identifying transient high-risk moments and enhancing operational safety during lifting tasks.

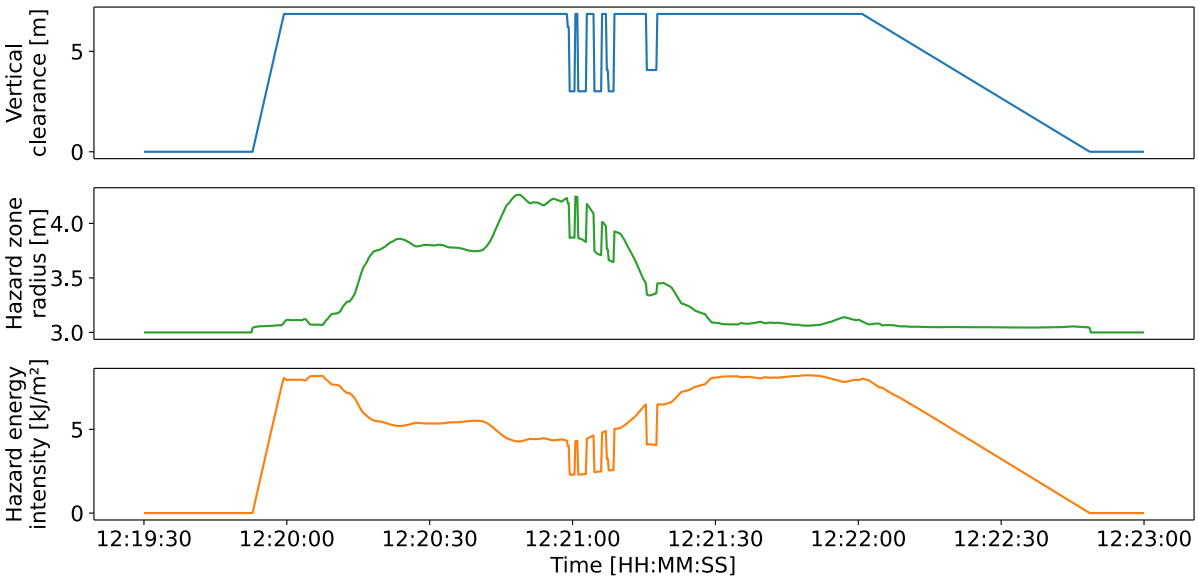

Figure 16: Vertical clearance, hazard zone radius, and hazard energy intensity during one lifting operation.

4.5 Evaluating site hazard energy distribution and incident severity

Once the hazard zones and energy values are determined for each lifting operation, a site-level hazard energy evaluation can be conducted. As shown in Figure 17, a hazard energy intensity heatmap was generated, summarizing where high-energy activities repeatedly occur on the site over the workday. The heatmap reveals spatial patterns of risk, with orange colors indicating zones with frequent or intense lifting hazards, which is over 1000 kJ·s/m^2. In contrast, other areas show a more diffuse distribution of hazard energy intensity, indicating that risks are spread over a broader area. Dark areas suggest safer zones, where the hazard energy is minimal or nonexistent. Safety measures such as restricted access areas can be implemented by identifying high-risk zones.

With high energy intensity distributed on the site, energy exposure received by workers is also determined by the incidents detected, where workers entered hazard zones during the lifting operations. Figure 18 shows the result of the incident detection over a day, where five workers were tracked. The upper panel shows the occurrence time and duration of incidents for each worker, while the lower panel shows the locations of all incidents. Most incidents occurred at the assembly area, while a few were at the hoisting locations.

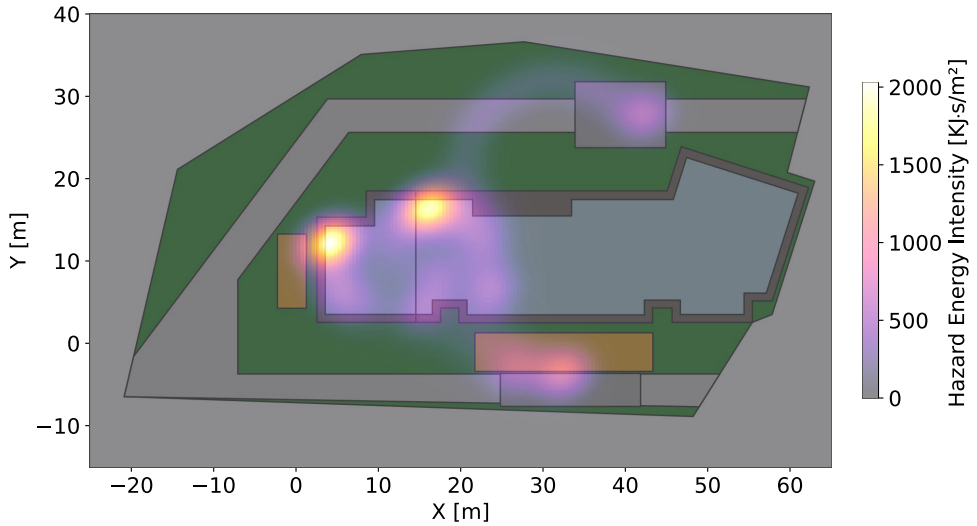

Figure 17: Hazard energy intensity (density) map of the site on one day.

Table 11 summarizes the incident count for each worker. Additionally, the result of the potential exposure of hazard energy to workers is presented. Worker 1, as rigger, with the highest incident count (63) and accumulated exposure (529.06 kJ·s), was exposed to both frequent and high-intensity hazard events, underscoring a potentially unsafe work environment or task assignment. Given that this is a relatively compact construction site, it was almost impossible to avoid such incidents; the operator had to traverse the work area for lifting. In contrast, Workers 4 and 5 had minimal exposure, suggesting lower-risk roles or more effective controls. This estimation not only quantifies exposure but also reveals meaningful differences in risk profiles, enabling data-driven interventions. By assessing both frequency and severity, this metric provides a more nuanced understanding of safety performance and supports targeted improvements in hazard management.

Incidents detected when no load was attached to the hook accounted for 50% of the total, significantly exaggerating the number of incidents compared to detection methods that incorporate the identification of lifting operations and their stages. Worker 2, rigger, was the most exposed to struck-by hazards. However, the precision of incident detection remains limited in terms of the hazard zone size, as it does not account for the geometry of the lifted elements.

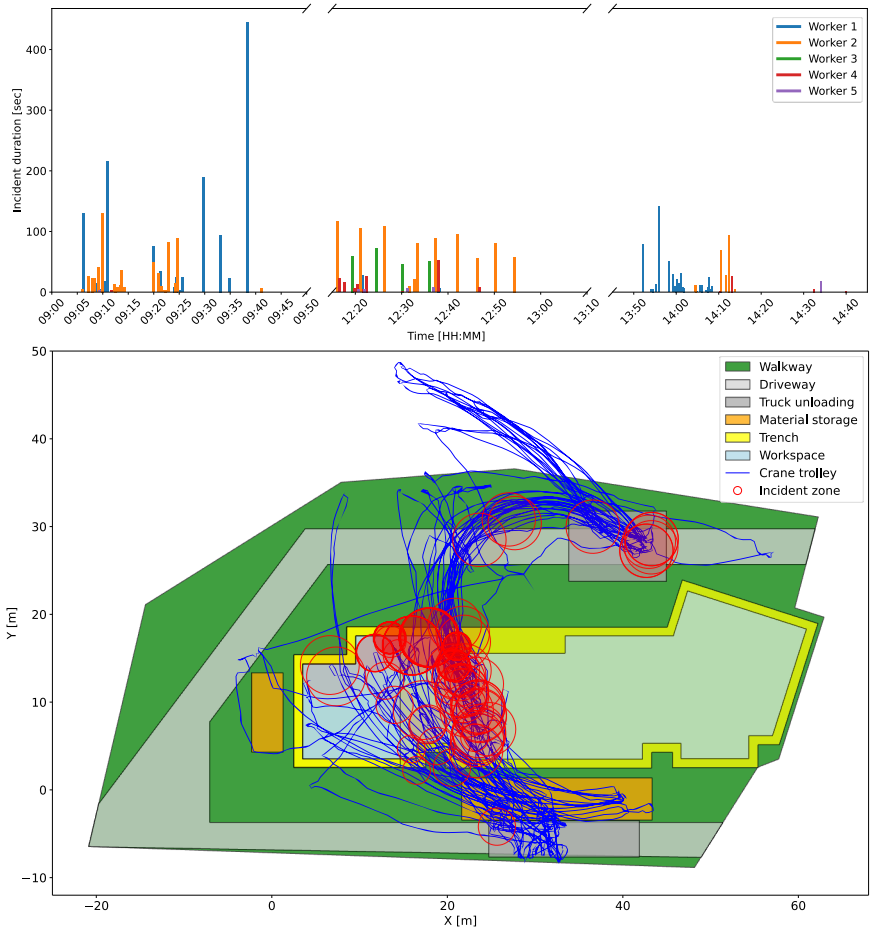

Figure 18: Results of incident detection on the site on a day: incident timestamp (upper) and locations (lower).

Table 11: Overview of hazard energy potential exposure of the tracked worker over the three days.

ID	Incident count [No]	Accumulated hazard energy exposure [kJ·s]	Maximum hazard energy exposure [kJ]
Worker 1	63	529.06	32.72
Worker 2	60	314.52	12.75
Worker 3	12	79.84	6.66
Worker 4	18	31.70	2.99
Worker 5	7	12.33	1.01

5. DISCUSSION

This study demonstrated the feasibility of using RTK-GNSS sensors mounted on a tower crane trolley monitoring lifting operations and estimating related hazards, including energy intensities and spatial distributions. By analyzing the trolley's vertical displacement, the system effectively detected crane activities, segmented lifting operations into distinct stages, and enabled hazard assessment. Therefore, the presented work shows a novel application of RTK-GNSS technology for characterizing real-world lifting operations. In addition, compared to traditional monitoring approaches, such as vision-based or multi-sensor systems, the proposed method offers several advantages. Vision-based methods are often sensitive to occlusion, lighting conditions, and require complex image processing, while multi-sensor systems typically involve higher installation and maintenance costs. In contrast, the RTK-GNSS-based approach enables direct and continuous measurement of crane motion with high spatial accuracy using a single sensing modality, reducing system complexity and improving robustness in outdoor construction environments. However, compared to methods that incorporate richer contextual or dynamic information, the proposed approach may be less effective in capturing complex dynamic behaviors.

The proposed framework and case study implementation addressed the research questions. First, the results confirmed that RTK-GNSS sensors alone can capture vertical and horizontal displacements with sufficient precision to detect and segment lifting operations (RQ1). Vertical displacement, particularly during hoisting and lowering, proved a reliable indicator of lifting activity, particularly for medium to heavy loads where the induced displacement is more pronounced. For light loads, however, the vertical displacement may be too small to be reliably detected, which limits the effectiveness of this approach. Second, vertical displacement data enabled the estimation of payload weight through machine learning models, which were validated against IFC model data of prefabricated components (RQ2). Third, by integrating crane trajectories with as-planned BIM models, the method facilitated the identification of lifted elements, approximation of their bounding box dimensions, and estimation of their weight. This integration allowed for energy-based calculation of hazard zones across lifting stages (RQ3). Finally, by combining hazard energy intensity and zone dimensions with worker location data (using RTK-GNSS wearables), the method supported spatial and temporal analysis of hazard energy exposure. Incident severity was quantified based on cumulative energy exposure when workers entered hazard zones, offering a scalable and practical framework for incident severity assessment (RQ4). It should be noted that, due to the use of conservative assumptions (e.g., bounding box approximations and simplified weight estimation), the resulting hazard energy exposure may be overestimated, providing a safety-oriented upper-bound assessment.

However, the proposed approach has several limitations. First, the accuracy of detecting lifting events depends on the magnitude of vertical displacement, which becomes less reliable for light payloads. Although velocity patterns can still indicate crane activity, minimal weight changes fall below the current sensitivity threshold (0.05 cm). Moreover, the use of static vertical displacement for estimating load weight does not account for dynamic factors such as oscillation or vertical acceleration, which can introduce noise or delay in classification. Future work may address this limitation by incorporating dynamic motion models or sensor fusion with IMUs or vision-based methods. Therefore, we regard estimated weight as a supplementary information for estimating the weight. It enables conservative and real-time energy estimates via weight classes, while IFC mass and geometry provide the precise post-lift ground truth. When lift schedule, sequence, or known element IDs are available, the matching accuracy improves further, and IFC values continue to calibrate and refine the estimator.

Currently, the height of the payload is inferred from the trolley position, as the RTK-GNSS sensor is mounted on the trolley rather than the hook. While this simplifies installation and ensures reliable signal quality, it introduces a source of estimation error. The error analysis relies on RTK-GNSS self-consistency without an independent reference. Future work should include other methods for ground truth validation, such as the use of a robotic total-station and (stereo-) vision cameras. Integrating computer vision, as proposed in (Chian et al., 2022), or using hook-mounted sensors could enhance the precision of payload height measurements. Additionally, the relationship between vertical displacement and payload weight was observed to be nonlinear and affected by crane structural characteristics (e.g., jib stiffness, connection geometry). While machine learning models (e.g., Random Forest and XGBoost) outperformed physics-based regression in predicting weight, incorporating crane-specific mechanical parameters—such as elastic modulus or counterweight dynamics—could refine this estimation. Importantly, it is not a single size that is inferred from weight; instead, we discretize mass into weight classes and use the class-specific worst-case projected dimensions from the IFC catalogue to compute conservative hazard envelopes.

The current model approximates payloads as rectangular bounding boxes and assumes cone-shaped hazard zones.

While this conservative method ensures safety, it may overestimate risk for irregular or lightweight elements. The use of detailed IFC-derived geometry and material properties can increase the granularity of hazard assessment and better support safety-critical decisions. As an exploratory study with limited training data, this simplification reflects practical constraints. Moreover, inferring dimensions from weight alone is insufficient for reliable deployment. In practice, combining weight estimation with the BIM model and the lifting schedule to identify the exact element can be adopted to better represent the hazard zone and energy potential. Finally, integrating this RTK-GNSS-based method with immersive visualization platforms like Virtual Reality (VR) offers significant promise. VR can simulate hazard energy exposure in real-time and support proactive path planning for workers and equipment. This could provide a user-centric interface for safety training and enhance real-time incident awareness (Speiser et al., 2024).

General Data Protection Regulation (GDPR) and data security issues may pose a severe limitation on implementing the complete framework and the respective technologies it uses on human labor. However, existing good practices already suggest potential avenues for solving important privacy issues and rights. The avenues involve applying additional data handling processes and technology. For example, certain categories of data (e.g., personal information) are neither captured nor stored; data is processed locally and deleted within short time frames; and only essential information is extracted and used in a fully anonymized form. It is recommended in the near future that relevant legal frameworks, best practices, and user-acceptance studies may assist the construction sector in adopting such technology.

6. CONCLUSION

This paper presented a framework for quantifying and visualizing struck-by hazard energy during tower crane lifting operations using a single RTK-GNSS sensor mounted on the trolley together with RTK-GNSS wearables carried by volunteering pedestrian construction workers. By leveraging centimeter-level positional accuracy, the system successfully detected lifting events, estimated payload weights based on vertical crane jib displacement. It integrated this information into as-planned building information models and construction schedules (4D BIM) and assessed it in the context of struck-by hazards. In this way, the proposed framework provides a lightweight, scalable, and data-driven alternative for hazard detection and incident analysis in tower crane operations.

The real-world case study demonstrated the practical applicability of the proposed framework. RTK-GNSS provided centimeter-level positioning accuracy for crane and worker tracking. For payload estimation, XGBoost achieved an RMSE of 246.58 kg, supporting reliable classification into predefined 500 kg weight intervals. The rule-based detector identified 59 of 89 annotated lifting operations, including 56 of 64 prefab-element lifts, with no false positives. In addition, 21 lifted elements were matched to prefab elements in the IFC model, and the highest accumulated hazard energy exposure reached 529.06 kJ·s for an individual worker.

Furthermore, this work contributed to the growing body of work supporting automated, energy-based design and planning of safe construction workplaces. The utilized energy-based hazard assessment framework enabled identification of dynamic hazard zones by considering both gravitational and kinetic energy across different operational stages. Using a combination of trajectory analysis and probabilistic modeling, the system visualized high-risk areas through hazard energy density maps and assessed potential pedestrian worker exposure using standardized thresholds articulated in the research literature. Several limitations were discovered, of which one is to conduct a long-term study that measures the impact on workplace safety performance. In the foreseeable future, the proposed technology may facilitate real-time safety monitoring and support proactive control in the field.

Therefore, this study introduces a practical method for crane hazard monitoring that balances simplicity and robustness. While several limitations exist and some have been pointed out, the findings lay the groundwork for future developments in data-driven safety systems, here for tower crane lifting operations leveraging the combination of RTK-GNSS tracking, 4D BIM integration, and energy-based risk models to protect pedestrian workers in dynamic and complex construction work environments.

ACKNOWLEDGEMENT

The research presented in this paper was funded by the EU Horizon 2020 research and innovation program under grant agreement nos. 958398 (BIM2TWIN) and 101058548 (BEEYONDERS). The authors thank Fira Oy and Sitedrive Oy for providing access to their construction site in Helsinki, Finland.

REFERENCES

Albert A., Hallowell M. R., & Kleiner B. M. (2014). Enhancing construction hazard recognition and communication with energy-based cognitive mnemonics and safety meeting maturity model: Multiple baseline study, Journal of Construction Engineering and Management, 140(2), 04013042, https://doi.org/10.1061/(ASCE)CO.1943-7862.0000790.

Ali A. H., Zayed T., Wang R. D., & Kit M. Y. S. (2024). Tower crane safety technologies: A synthesis of academic research and industry insights, Automation in Construction, 163, 105429, https://doi.org/10.1016/j.autcon.2024.105429.

American Society of Mechanical Engineers (ASME). (2012). Safety standard for cableways, cranes, derricks, hoists, hooks, jacks, and slings, ASME, https://www.asme.org/getmedia/52b15c28-c56a-4889-89a9-32223b7bdd83/35936.pdf (accessed April 15, 2025).

Bayona A., Hallowell M. R., Bhandari S., Moyen N., & Lien A. (2025). Impact of energy-based safety training on quality of prejob safety meetings and control of hazardous energy in construction: Multiple baseline experiment, Journal of Construction Engineering and Management, 151(3), 04025086, https://doi.org/10.1061/JCEMD4.COENG-15563.

Bishop C. M. (2006). Pattern recognition and machine learning, Springer, ISBN 9780387310732, https://www.microsoft.com/en-us/research/wp-content/uploads/2006/01/Bishop-Pattern-Recognition-and-Machine-Learning-2006.pdf (accessed April 15, 2025).

Breloff S. P., Garza C. E., Brogan A., Bunting J., Trout D., Pena M., & Earnest G. S. (2023). Struck-by injuries in the construction sector: Common hazards, barriers, and opportunities to keep workers safe, NIOSH Science Blog, https://blogs.cdc.gov/niosh-science-blog/2023/04/04/2023-struck-by-stand-down/ (June 10, 2025).

Bureau of Labor Statistics (BLS). (2019). Fatal occupational injuries involving cranes, 2011–2017, U.S. Bureau of Labor Statistics, https://www.bls.gov/iif/factsheets/fatal-occupational-injuries-cranes-2011-17 (accessed November 28, 2024).

Bureau of Labor Statistics (BLS). (2024). Census of fatal occupational injuries summary, 2023, U.S. Bureau of Labor Statistics, https://www.bls.gov/news.release/cfoi.nr0.htm (accessed February 28, 2025).

Carmona A. M., Chaparro A. I., Pardo S., Velásquez R., Botero-Valencia J., Castano-Londono L., Marquez-Viloria D., Botero C., & Mesa A. M. (2019). A low-cost system for monitoring tower crane productivity cycles combining inertial measurement units, load cells and LoRa networks, in: Proceedings of the 35th CIB W78 2018 Conference, pp. 677–684, https://doi.org/10.1007/978-3-030-00220-6_81.

Cheng T., Venugopal M., Teizer J., & Vela P. A. (2011). Performance evaluation of ultra wideband technology for construction resource location tracking in harsh environments, Automation in Construction, 20(5), 1173–1184, https://doi.org/10.1016/j.autcon.2011.05.001.

Cheng T., & Teizer J. (2014). Modeling tower crane operator visibility to minimize the risk of limited situational awareness, Journal of Computing in Civil Engineering, 28(4), 04014004, https://doi.org/10.1061/(ASCE)CP.1943-5487.0000282.

Chian E. Y. T., Goh Y. M., & Tian J. (2022). Dynamic identification of crane load fall zone: A computer vision approach, Safety Science, 156, 105904, https://doi.org/10.1016/j.ssci.2022.105904.

Costin A. M., & Teizer J. (2015). Fusing passive RFID and BIM for increased accuracy in indoor localization, Visualization in Engineering, 3(1), 17, https://doi.org/10.1186/s40327-015-0030-6.

Danel T., Lafhaj Z., Puppala A., Lienard S., & Richard P. (2021). Proposal for tower crane productivity indicators based on data analysis in the era of Construction 4.0, Buildings, 11(1), 21, https://doi.org/10.3390/buildings11010021.

Danel T., Lafhaj Z., Puppala A., BuHamdan S., Lienard S., & Richard P. (2024). Identifying tower crane activities with data: The case of the concrete pouring, Engineering, Construction and Architectural Management, 31(4), 939–956, https://doi.org/10.1108/ECAM-10-2021-0936.

Devesse W. (2012). Slew control methods for tower cranes, KTH Royal Institute of Technology, thesis report, https://www.diva-portal.org/smash/get/diva2:541819/FULLTEXT01.pdf (accessed April 15, 2025).

Emlid. (2024). Reach M2 RTK GNSS receiver & GPS module, https://emlid.com/reach/ (September 20, 2024).

Eurostat. (2024). Accidents at work – statistics by economic activity, Eurostat Statistics Explained, https://ec.europa.eu/eurostat/statistics-explained/index.php?title=Accidents_at_work_-_statistics_by_economic_activity (accessed June 11, 2024).

Fang Y., & Cho Y. K. (2015). Crane load positioning and sway monitoring using an inertial measurement unit, in: Proceedings of the 2015 International Workshop on Computing in Civil Engineering, pp. 700–707, https://doi.org/10.1061/9780784479247.087.

Fang Y., Chen J., Cho Y. K., Kim K., Zhang S., & Perez E. (2018). Vision-based load sway monitoring to improve crane safety in blind lifts, Journal of Structural Integrity and Maintenance, 3(4), 233–242, https://doi.org/10.1080/24705314.2018.1531348.

Federal Emergency Management Agency (FEMA). (2008). FEMA national US&R response system structural collapse technician, module 4 – lifting and rigging, FEMA, https://www.fema.gov/pdf/emergency/usr/module4.pdf (accessed April 15, 2025).

Fleming, M., & Fischer B. (2017). Hazard recognition: Bridging knowledge and competency for process and occupational safety, Professional Safety, 52-61, http://onepetro.org/PS/article-pdf/62/06/52/2179622/asse-17-06-52.pdf (accessed March 20, 2026).

Golovina O., Teizer J., & Pradhananga N. (2016). Heat map generation for predictive safety planning: Preventing struck-by and near miss interactions between workers-on-foot and construction equipment, Automation in Construction, 71, 99–115, https://doi.org/10.1016/j.autcon.2016.03.008.

Haddon W., Jr. (1968). The changing approach to the epidemiology, prevention, and amelioration of trauma: The transition to approaches etiologically rather than descriptively based, American Journal of Public Health, 58(8), 1431–1438, https://doi.org/10.2105/ajph.58.8.1431.

Haddon, W. Jr. (1970). On the escape of tigers: An ecologic note. *Technology Review*, 45-47.

Hallowell M. R., Alexander D., & Gambatese J. A. (2017). Energy-based safety risk assessment: Does magnitude and intensity of energy predict injury severity?, Construction Management and Economics, 35(1–2), 64–77, https://doi.org/10.1080/01446193.2016.1274418.

Hong K., & Teizer J. (2024). Automated construction site safety monitoring using preidentified static and dynamic hazard zones, in: Proceedings of the 41st International Symposium on Automation and Robotics in Construction (ISARC), pp. 388–395, https://doi.org/10.22260/ISARC2024/0051.

Hong, K., & Teizer, J. (2025). "Digital construction site layout planning and real-time trajectory analysis for proactive safety monitoring and control of struck-by hazards", Automation in Construction, 177, 106353, https://doi.org/10.1016/j.autcon.2025.106353

Hu S., Fang Y., & Guo H. (2021). A practicality and safety-oriented approach for path planning in crane lifts, Automation in Construction, 127, 103695, https://doi.org/10.1016/j.autcon.2021.103695.

Hu S., Fang Y., & Moehler R. (2023). Estimating and visualizing the exposure to tower crane operation hazards on construction sites, Safety Science, 160, 106044, https://doi.org/10.1016/j.ssci.2022.106044.

Hu S., Wang J., & Fang Y. (2024). Semantic Web–assisted progress monitoring of crane operations in construction projects, Proceedings of the ICE – Smart Infrastructure and Construction, pp. 1–10, https://doi.org/10.1680/jsmic.24.00011.

Hwang S. (2012). Ultra-wide band technology experiments for real-time prevention of tower crane collisions, Automation in Construction, 22, 545–553, https://doi.org/10.1016/j.autcon.2011.11.015.

IfcOpenShell. (2024). IfcOpenShell – The open source IFC toolkit and geometry engine, https://ifcopenshell.org/ (accessed June 17, 2024).

International Organization for Standardization (ISO). (2005). Cranes — Safe use — Part 3: Tower cranes, ISO 12480-3, https://www.iso.org/standard/72671.html (accessed April 15, 2025).

Jiang W., & Ding L. (2024). Unsafe hoisting behavior recognition for tower crane based on transfer learning, Automation in Construction, 160, 105299, https://doi.org/10.1016/j.autcon.2024.105299.

Johansen K. W., Hong K., Schultz C., & Teizer J. (2024a). Automated quantification of construction workers' exposure to falling object hazards, Proceedings of the ICE – Management, Procurement and Law, pp. 1–16, https://doi.org/10.1680/jmapl.23.00103.

Johansen K. W., Teizer J., & Schultz C. (2024b). Automated rule-based safety inspection and compliance checking of temporary guardrail systems in construction, Automation in Construction, 168, 105849, https://doi.org/10.1016/j.autcon.2024.105849.

Kang S., & Miranda E. (2004). Physics based model for simulating the dynamics of tower cranes, in: Proceedings of the 10th International Conference on Computing in Civil and Building Engineering, https://doi.org/10.25643/bauhaus-universitaet.240.

Kusznir T., & Smoczek J. (2023). Soft-computing-based estimation of a static load for an overhead crane, Sensors, 23(13), 5842, https://doi.org/10.3390/s23135842.

Marks E. D., Wetherford J. E., Teizer J., & Yabuki N. (2013). Potential of leading indicator data collection and analysis for proximity detection and alert technology in construction, in: Proceedings of the 30th International Symposium on Automation and Robotics in Construction (ISARC), pp. 1029–1036, https://doi.org/10.22260/ISARC2013/0113.

Milazzo M. F., Ancione G., Brkic V. S., & Vališ D. (2016). Investigation of crane operation safety by analysing main accident causes, in: Proceedings of Risk, Reliability and Safety: Innovating Theory and Practice (ESREL 2016), pp. 74–80, https://doi.org/10.1201/9781315374987.

Nadar M. A., Awakian C. A., & Khoury H. K. (2013). An intelligent system for monitoring tower cranes on construction sites, in: Proceedings of the 30th International Symposium on Automation and Robotics in Construction (ISARC), pp. 1239–1246, https://doi.org/10.22260/ISARC2013/0139.

Ning X., Qi J., & Wu C. (2018). A quantitative safety risk assessment model for construction site layout planning, Safety Science, 104, 246–259, https://doi.org/10.1016/j.ssci.2018.01.016.

Nishizawa Y., & Mishima M. (2024). Acquisition of tower crane operational performance using hook mounted RTK positioning and image recognition, in: Proceedings of the Creative Construction Conference 2024, pp. 1–10, https://doi.org/10.3311/CCC2024-030.

Occupational Safety and Health Administration (OSHA). (2014). Small entity compliance guide for the final rule for cranes and derricks in construction, OSHA, https://www.osha.gov/sites/default/files/publications/OSHA3433.pdf (accessed April 15, 2025).

Occupational Safety and Health Administration (OSHA). (2019). Using leading indicators to improve safety and health outcomes, OSHA, https://www.osha.gov/sites/default/files/publications/OSHA_Leading_Indicators.pdf (April 15, 2025).

Occupational Safety and Health Administration (OSHA). (2024). Accident search results, OSHA, https://www.osha.gov/ords/imis/accidentsearch.search (accessed November 28, 2024).

Park J., Kim K., & Cho Y. K. (2017). Framework of automated construction-safety monitoring using cloud-enabled BIM and BLE mobile tracking sensors, Journal of Construction Engineering and Management, 143(2), 05016019, https://doi.org/10.1061/(ASCE)CO.1943-7862.0001223.

Pfitzner F., Braun A., & Borrmann A. (2023). Towards data mining on construction sites: Heterogeneous data acquisition and fusion, in: Proceedings of ECPPM 2022 – eWork and eBusiness in Architecture, Engineering and Construction, pp. 516–524, https://doi.org/10.1201/9781003354222-66.

Pradhananga N., & Teizer J. (2013). Automatic spatio-temporal analysis of construction site equipment operations using GPS data, Automation in Construction, 29, 107–122, https://doi.org/10.1016/j.autcon.2012.09.004.

Rao A. S., Radanovic M., Liu Y., Hu S., Fang Y., Khoshelham K., Palaniswami M., & Ngo T. (2022). Real-time monitoring of construction sites: Sensors, methods, and applications, Automation in Construction, 136, 104099, https://doi.org/10.1016/j.autcon.2021.104099.

Rashid K. M., & Louis J. (2020). Automated activity identification for construction equipment using motion data from articulated members, Frontiers in Built Environment, 5, 144, https://doi.org/10.3389/fbuil.2019.00144.

Rauscher F., & Sawodny O. (2017). An elastic jib model for the slewing control of tower cranes, IFAC-PapersOnLine, 50(1), 9796–9801, https://doi.org/10.1016/j.ifacol.2017.08.886.

Sacks R., Navon R., Brodetskaia I., & Shapira A. (2005). Feasibility of automated monitoring of lifting equipment in support of project control, Journal of Construction Engineering and Management, 131(5), 604–614, https://doi.org/10.1061/(ASCE)0733-9364(2005)131:5(604).

Sacks R., Brilakis I., Pikas E., Xie M., & Girolami M. (2020). Construction with digital twin information systems, Data-Centric Engineering, 1, e14, https://doi.org/10.1017/dce.2020.16.

Sherafat B., Ahn C. R., Akhavian R., Behzadan A. H., Golparvar-Fard M., Kim H., Lee Y.-C., Rashidi A., & Azar E. R. (2020). Automated methods for activity recognition of construction workers and equipment: State-of-the-art review, Journal of Construction Engineering and Management, 146(6), 03120002, https://doi.org/10.1061/(ASCE)CO.1943-7862.0001842.

Shi H., Huang J., Bai X., Huang X., & Sun J. (2021). Nonlinear anti-swing control of underactuated tower crane based on improved energy function, International Journal of Control, Automation and Systems, 19(12), 3967–3982, https://doi.org/10.1007/s12555-020-0292-1.

Speiser K., & Teizer J. (2024a). Formalizing virtual construction safety training: a schematic data framework enabling real-world hazard simulations using BIM and location tracking. Journal of Information Technology in Construction, 29. https://doi.org/10.36680/j.itcon.2024.043.

Speiser K., & Teizer J. (2024b). Worker-centric path planning: Simulating hazardous energy to control construction safety using graph theory, in: Proceedings of the 41st International Symposium on Automation and Robotics in Construction (ISARC), pp. 505–512, https://doi.org/10.22260/ISARC2024/0066.

Speiser K., Teizer J., & Ali G. M. (2024). Smart signalperson for safe tower crane operations on a future digital construction site, in: Proceedings of Joint Safety, Health, and Well-Being in Construction (W099) and People in Construction (W123) International Conference — 2024, pp. 353–365, ISBN 9789988391386, https://orbit.dtu.dk/en/publications/smart-signalperson-for-safe-tower-crane-operations-on-a-future-di.

Teizer J., & Cheng T. (2015). Proximity hazard indicator for workers-on-foot near miss interactions with construction equipment and geo-referenced hazard areas, Automation in Construction, 60, 58–73, https://doi.org/10.1016/j.autcon.2015.09.003.

Teizer J., Johansen K. W., Schultz C. L., Speiser K., Hong K., & Golovina O. (2024). A digital twin model for advancing construction safety, in: Proceedings of International Conference on Construction Logistics, Equipment, and Robotics (CLEaR 2023), pp. 201–212, https://doi.org/10.1007/978-3-031-44021-2_22.

Wielgocka N., Hadas T., Kaczmarek A., & Marut G. (2021). Feasibility of using low-cost dual-frequency GNSS receivers for land surveying, Sensors, 21(6), 1956, https://doi.org/10.3390/s21061956.

Xiong C., & Niu Y. (2019). Investigation of the dynamic behavior of a super high-rise structure using RTK-GNSS technique, KSCE Journal of Civil Engineering, 23(2), 654–65, https://doi.org/10.1007/s12205-018-0238-9

Yang J., Vela P., Teizer J., & Shi Z. (2014). Vision-based tower crane tracking for understanding construction activity, Journal of Computing in Civil Engineering, 28(1), 103–112, https://doi.org/10.1061/(ASCE)CP.1943-5487.0000242.

Yong Y. P., Lee S. J., Chang Y. H., Lee K. H., Kwon S. W., Cho C. S., & Chung S. W. (2023). Object detection and distance measurement algorithm for collision avoidance of precast concrete installation during the crane lifting process, Buildings, 13(10), 2551, https://doi.org/10.3390/buildings13102551.

Zhang Q., Mei B., Yang H., Hu X., An W., Yue Y., Xu Y., & Wang Z. (2025). Stress measurement and analysis of structural parameters of flat arm tower crane under different working conditions, Buildings, 15(7), 1137, https://doi.org/10.3390/buildings15071137.

Zhao L., Liu Z., & Mbachu J. (2019). Development of intelligent prefabs using IoT technology to improve the performance of prefabricated construction projects, Sensors, 19(19), 4131, https://doi.org/10.3390/s19194131.

Zhong D., Lv H., Han J., & Wei Q. (2014). A practical application combining wireless sensor networks and Internet of Things: Safety management system for tower crane groups, Sensors, 14(8), 13794–13814, https://doi.org/10.3390/s140813794.